ERDC/CRREL TR-22-9

Cold Regions Research
and Engineering Laboratory

US Army Corps
of Engineers®
Engineer Research and
Development Center

ERDC
ENGINEER RESEARCH & DEVELOPMENT CENTER

Understanding and Improving Snow Processes in Noah-MP over the Northeast United States via the New York State Mesonet

Theodore W. Letcher, Justin R. Minder, and Patrick Naple

August 2022

The U.S. Army Engineer Research and Development Center (ERDC) solves the nation's toughest engineering and environmental challenges. ERDC develops innovative solutions in civil and military engineering, geospatial sciences, water resources, and environmental sciences for the Army, the Department of Defense, civilian agencies, and our nation's public good. Find out more at www.erdc.usace.army.mil.

To search for other technical reports published by ERDC, visit the ERDC online library at https://erdclibrary.on.worldcat.org/discovery.

ERDC/CRREL TR-22-9
August 2022

Understanding and Improving Snow Processes in Noah-MP over the Northeast United States via the New York State Mesonet

Theodore W. Letcher

U.S. Army Engineer Research and Development Center (ERDC)
Cold Regions Research and Engineering Laboratory (CRREL)
72 Lyme Road
Hanover, NH 03755-1290

Justin R. Minder, Patrick Naple

University at Albany, State University of New York
1400 Washington Ave.
Albany, New York 12222

Final Report

Prepared for National Oceanic and Atmospheric Administration
1401 Constitution Avenue NW, Room 5128
Washington, DC 20230

Under Project NA19OAR4590203

Abstract

Snow is a critical component of the global hydrologic cycle and is a key input to river and stream flow forecasts. In 2016, the National Oceanic and Atmospheric Administration launched the National Water Model (NWM) to provide a high-fidelity numerical forecast of streamflow integrated with the broader atmospheric prediction modeling framework. The NWM is coupled to the atmospheric model using the Noah-MP land surface modeling framework. While snow in Noah-MP has been consistently evaluated in the western United States, less attention has been paid to understanding and optimizing its performance in the Northeast US (NEUS). The newly installed New York State Mesonet (NYSM), a network of high-quality surface meteorological stations distributed across New York State, provides a unique opportunity to evaluate Noah-MP performance in the NEUS. In this report, we document the methodology used to perform single-column simulations using meteorological inputs from the NYSM and compare the point evaluations against baseline NWM performance. We further discuss how enhanced surface energy balance measurements at a selection of NYSM sites can be used to evaluate specific components of Noah-MP and present initial results.

Contents

Figures and Tables

Figures

Tables

Preface

This study was conducted for the National Oceanic and Atmospheric Administration under Project NA19OAR4590203, "Improving Snow and Streamflow Simulation in the National Water Model by Leveraging Advanced Mesonet Observations from the Northeastern United States."

This research was made possible by the New York State (NYS) Mesonet. Original funding for the NYS Mesonet was provided by Federal Emergency Management Agency grant FEMA-4085-DR-NY, with the continued support of the NYS Division of Homeland Security & Emergency Services; the state of New York; the Research Foundation for the State University of New York (SUNY); the University at Albany, SUNY; the Atmospheric Sciences Research Center (ASRC) at SUNY Albany; and the Department of Atmospheric and Environmental Sciences (DAES) at SUNY Albany.

The work was performed by the University at Albany, State University of New York; and the Terrestrial and Cryospheric Sciences Branch of the Research and Engineering Division, U.S. Army Engineer Research and Development Center, Cold Regions Research and Engineering Laboratory (ERDC-CRREL). At the time of publication, Dr. John Weatherly was Branch Chief, and Dr. Caitlin A. Callaghan was Division Chief. The Acting Deputy Director of ERDC-CRREL was Mr. Bryan E. Baker, and the Director was Dr. Joseph L. Corriveau.

COL Christian Patterson was Commander of ERDC, and Dr. David W. Pittman was Director.

Acronyms and Abbreviations

AORC	Analysis of Record for Calibration
BATS	Biosphere Atmosphere Transfer Scheme
CLASS	Canadian Land Surface Scheme
CONUS	Continental United States
HRRR	High Resolution Rapid Refresh
LSM	Land Surface Model
LW	Longwave
LWC	Liquid Water Content
NEUS	Northeast United States
NIR	Near Infrared
NOAA	National Oceanic and Atmospheric Administration
Noah-MP	Noah Land Surface Model with Multi-Parameterization
NWM	National Water Model
NYSM	New York State Mesonet
QC	Quality Control
RMSE	Root Mean Square Error
RRTMG	Rapid Radiative Transfer Model
SEB	Surface Energy Budget
SWE	Snow Water Equivalent
WRF	Weather Research and Forecast

1 Introduction

In 2016, the National Oceanic and Atmospheric Administration (NOAA) started using a fully integrated hydrologic model, called the National Water Model (NWM), to aid in streamflow forecasting across the continental United States (CONUS). The core of this framework is the Weather Research and Forecast Hydrological modeling system (WRF-Hydro), which combines several disparate physical models that simulate the different parts of the hydrologic cycle (e.g., weather, snow, runoff, and streamflow) into a single unified model.

In this study, we focus on snow, which is a critical component of the hydrologic cycle and a major source of runoff in many regions throughout CONUS. Snow accumulation and melt impact soil moisture and runoff, which in turn impact the streamflow and water resource availability. Accordingly, the accuracy of simulated streamflow in the NWM is highly dependent on the accuracy of the snow model component. The NWM uses the Noah land surface model with multiple parameterization options (Noah-MP) land surface model (LSM) to simulate land processes, including snow. Numerous studies have focused on evaluating and calibrating snow processes in Noah-MP over the western United States, in particular over the Sierra Nevada and Colorado Plateau (e.g., Wrzesien et al. 2015; Minder et al. 2016; You et al. 2020). A less well-studied region for snow is that of the Northeastern United States (NEUS). Recently, a state-of-the-art network of surface meteorological monitoring stations covering New York State was brought online with the aim of improving weather forecast skill in the NEUS region. This network, the New York State Mesonet (NYSM: Brotzge et al. 2020) comprises 126 stations and is unique among similar networks as it measures snow in addition to standard meteorological variables. In this study, we leverage this network to evaluate snow processes within the Noah-MP LSM to better understand its performance in the NEUS.

1.1 Background

Numerous research efforts are underway to improve NWM performance across the country, with focuses on model evaluation, improving regionally variable tuning parameters, and data assimilation. While this study does not aim to directly improve the NWM, it sets the stage for future

improvements by evaluating snow performance in Noah-MP in a geographic region that is often overlooked in snow modeling research and calibration.

While typically not as deep or persistent as the high mountain snows in the western United States, snow is an integral part of the NEUS hydrologic cycle. For instance, mountain snow stored in the Catskill mountains of New York State make up a substantial portion of the New York City water supply (Matonse et al. 2011). Furthermore, snow in the NEUS is somewhat unique in that a variety of different snow types coexist in close proximity to each other. For example, transient maritime snowpacks are common in the southeastern coastal areas, while persistent alpine snowpacks exist in the nearby interior mountains in New York, Vermont, New Hampshire, and Maine. Additionally, lake-effect snow squalls that commonly develop downwind of the Eastern Great Lakes can build deep snowpacks in narrow geographic belts in western and central New York. Finally, snow in the NEUS is episodically impacted by broad, regional midwinter warming and rain-on-snow events creating ice lenses within the snowpack that modify the snowpack's thermal conductivity (e.g, Yen et al. 1991; Sturm and Perovich 2002), water retention capacity, and albedo (Albert and Perron 2000). The impact of these events on Noah-MP's snow model performance has not been robustly evaluated.

1.2 Objective

The primary objective of this research is to use the continuous measurements collected by the NYSM to evaluate simulated snow processes in the Noah-MP LSM over New York State. We also perform additional simulation studies to assess the sensitivity of Noah-MP to its snow-related internal configuration settings and tuning parameters. Furthermore, we provide recommendations to enhance Noah-MP simulation performance in the NEUS region.

1.3 Approach

We perform single-column ("point") Noah-MP simulations for each site within the NYSM using the meteorological measurements recorded at individual stations as the model input forcing. The model output is then compared to the measured snow depth at each site to evaluate model performance. Sensitivity experiments varying the precipitation phase partitioning method are performed to understand how one source of input

forcing uncertainty impacts the simulated snow. Enhanced model evaluations that include snow water equivalent and surface energy budget measurements are performed at NYSM sites.

By forcing the model with meteorological inputs from the data measured by the NYSM and evaluating the specific pieces of the surface energy balance over snow, we aim to better understanding how well Noah-MP simulates the individual physical processes that control snow accumulation and ablation in the NEUS.

1.4 Scope

The purpose of this report is to document the methodology used to perform and evaluate point simulations with Noah-MP using data from the NYSM and to discuss preliminary results.

2 Data and Methods

2.1 New York State Mesonet

The NYSM is a state-of-the-art network of 126 high-quality surface weather observing stations distributed evenly across New York State (Figure 1). Each site measures standard meteorological variables using high-quality calibrated instrumentation (Table 1). Refer to Brotzge et al. (2020) for a full description of the NYSM, including siting procedures, quality control (QC) methods, and sources of error. In addition to the standard meteorological variables collected at most automated weather stations (i.e., temperature, humidity, wind, pressure, and precipitation), each site also records incoming solar radiation, snow depth, and column soil properties (temperature and moisture). Snow depth is measured using a Campbell Scientific SR50A acoustic snow sensor. All measured variables are output at 5-minute intervals, providing a high temporal resolution dataset at each site.

Figure 1. Regional map showing the locations of each NYSM site. Topography is shaded for illustration purposes. Starred outlines indicate a snow site. Diamond outlines indicate a flux site. Labeled sites are examined in greater detail.

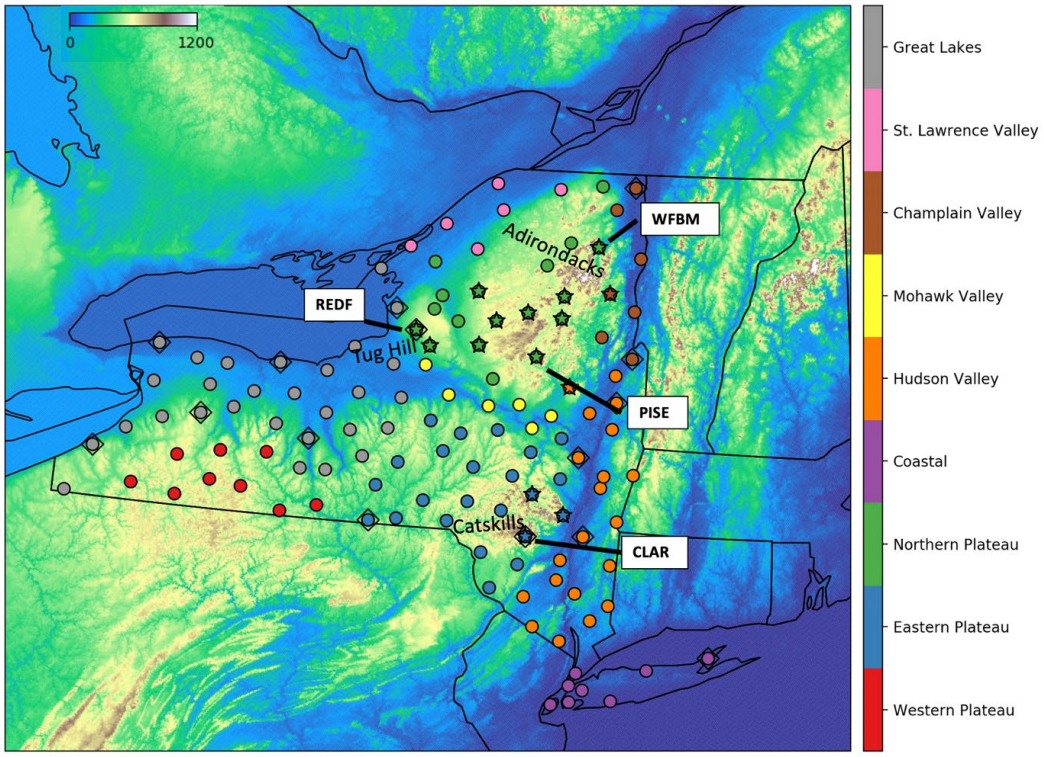

Table 1. Standard instruments at each NYSM site.

Variable	Instrument
2 Meter Temperature	RM Young 41342 fast response air temperature sensor
2 Meter RH	Vaisala HMP155 HUMICAP® humidity and temperature probe
Incoming Solar	LI-COR LI-200R Pyranometer
Windspeed/Direction	Lufft V200A Sonic anemometer if available, otherwise from an RM Young 05108 propeller anemometer
Rainfall/Precipitation	OTT Pluvio² mass precipitation gauge with double alter shield
Surface Pressure	Vaisala PTB330 silicon capacitive, absolute pressure sensor
Snow depth	SR50A mounted over a ridged white bored
Soil Moisture / Temperature	Stevens Hydraprobe III at 5, 25, and 50 cm depth

At all sites, the SR50A is mounted above a white rigid snow board to limit the contamination of vegetation on the measurement. The acoustic snow depth sensor is subject to significant high frequency noise, particularly during precipitation. As a result, the snow depth data are quality controlled by first removing any value where the measure snow depth is less than zero. Time-based interpolation techniques are then used to replace missing data gaps, and a daily running average is applied to the original 5 min data to smooth out high frequency noise.

Soil temperature and moisture are measured at 5, 25, and 50 cm depths using a Stevens Hydra-Probe II. Figure 2 shows an annotated photograph of a typical NYSM site.

Of the 126 sites, 20 sites are designated as specific “snow” sites, which include additional instrumentation to measure snow water equivalent (SWE). These sites are located in the Adirondack and Catskill mountains, as well as the on the Tug Hill Plateau east of Lake Ontario. SWE is measured using a Campbell Scientific CS725 gamma ray sensor that relates ground-sourced gamma radiation attenuated by the snowpack to SWE (Figure 3).

NYSM Surface Energy Budget (SEB) Sites

An additional 17 sites within the network have specialized instrumentation to measure the components that make up the surface energy budget (SEB). Specifically, these sites measure the net radiation, ground flux, and turbulent fluxes. The net radiation is measured using upward- and

downward-facing Kipp and Zonen CNR4 pyranometers and pyrgeometers, respectively. A closed-path eddy-covariance system is used to measure turbulent sensible and latent heat fluxes. This system includes a three-dimensional Campbell Scientific CSAT3A ultrasonic anemometer and a closed-path CO_2/H_2O gas analyzer installed approximately 8 m above ground level (AGL). The ground heat flux is measured at 6 cm deep using four Hukseflux HFP01 thermopiles that measure the temperature difference across the ceramics-plastic composite body of HFP01.

Figure 2. Annotated photograph of the site at Redfield, New York, taken during the spring.

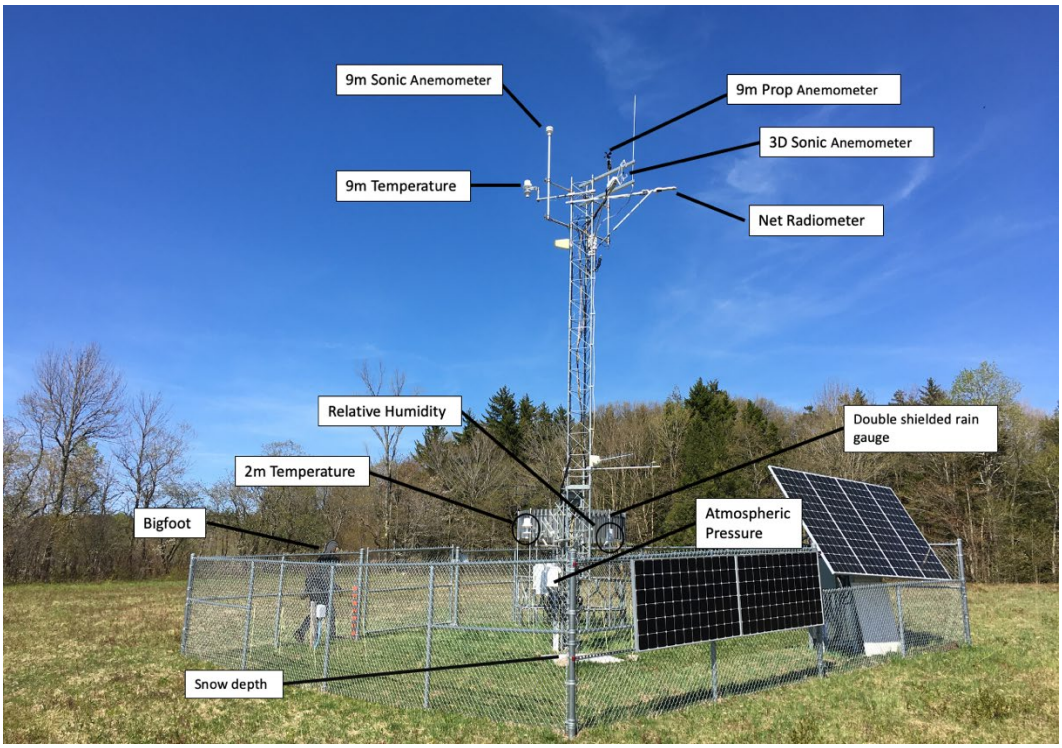

All the SEB data undergo basic quality control and are flagged under certain criteria. For instance, the net shortwave radiation flux is flagged if the upwelling shortwave flux is greater than the downwelling. An additional constraint is placed on the albedo measurement such that the albedo measurement is discarded anytime the measured downwelling shortwave radiation is less than 30 W m^{-2}. Additional checks are performed to flag times where moisture may be condensing on the pyrgeometers and causing errors in the longwave flux measurements. The turbulent flux measurements undergo robust quality control. In particular, each measurement is assigned a quality grade flag ranging from 1–9 that assesses the confidence in the turbulent flux measurement, with a value of 1 indicating high confidence and a value of 9 indicating no confidence

(Covert 2019). In this analysis, any flux measurement with a quality grade greater than 3 is discarded.

Figure 3. SWE monitoring station at Redfield, New York. Note that an additional snow depth sensor is placed here to monitor SWE and snow depth adjacently.

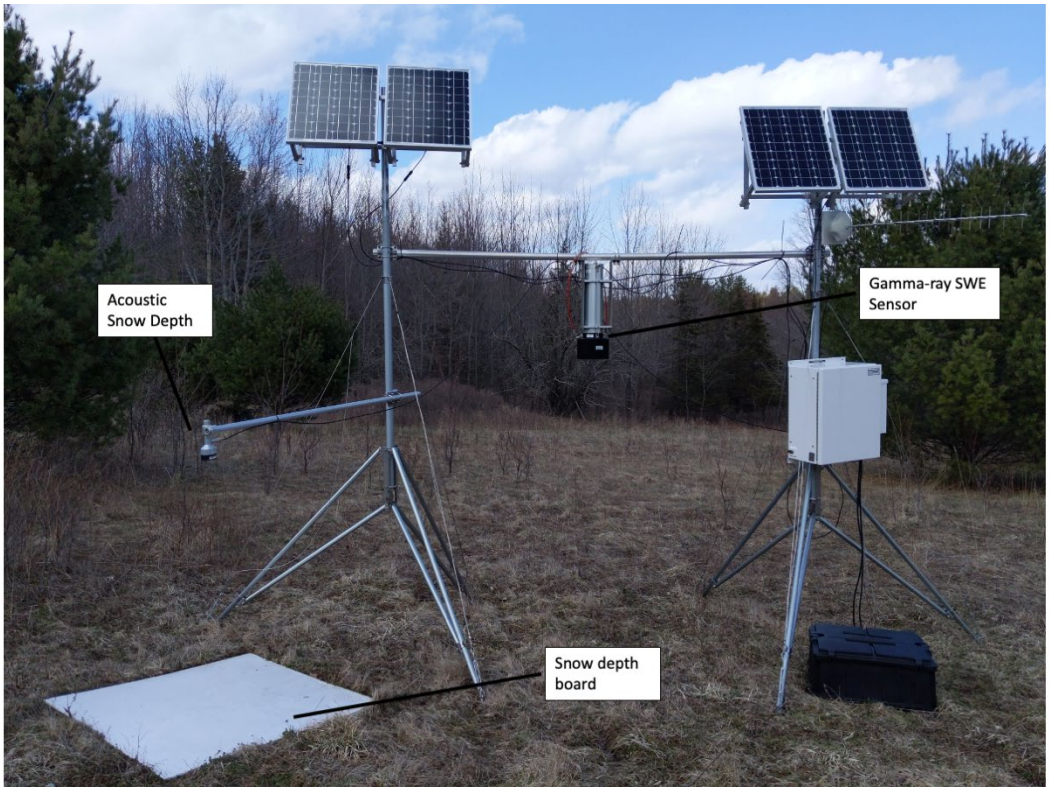

To retain a focus on snow, all flux measurements are discarded where the measured or modeled snow depth is less than 5 cm. For the comparison between the simulated and measured surface temperature, the Noah-MP output variable "TRAD" corresponding to the surface radiative temperature is used, matching the surface temperature measurement, which is derived from the upwelling LW radiative flux. Finally, all of the flux data are averaged into 30-minute intervals.

While the SEB data are a valuable tool for model validation, additional considerations are required when interpreting all components of the SEB data. For instance, the net radiometer is situated at approximately 9 m AGL on a boom that extends approximately 1.7 m out from the tower (e.g., Figure 2). This indicates that the downward facing pyranometer and pyrgeometer are measuring radiation not only from the surface but also from the infrastructure of the NYSM site, including, for example, the tower, instrumentation, and solar panels. Additional contamination

includes possible impacts from nearby forest elements. Under snow-covered conditions, this contamination likely causes the radiometers to measure a lower overall surface albedo and a higher surface radiative temperature than the actual snow surface.

The turbulent flux measurements are also subject to degradation during the winter months. In particular, the power-intensive 3D anemometers are often disabled during midwinter to conserve power consumption when the solar panels are less effective at power generation. As a result, the turbulent fluxes are only available for approximately 50–60% of the time during meteorological winter. For instance, less than 33% of measurements at the Redfield SEB site are of high enough quality for model validation (Covert 2019). An additional complication impacting the comparison between observed and simulated turbulent fluxes is associated with the "flux footprint." The flux footprint is essentially a mean land-cover classification–based climatological fetch and land-cover classification of the local terrain (Covert 2019). This complicates our evaluation process because roughness lengths used by the model to incorporate surface drag effects on airflow are based on snow cover and the prescribed land-cover class for the location. However, roughness lengths diagnosed for the monitoring stations represent mixed land classifications that fall within the flux footprint. For example, while the measured precipitation, snow depth, and solar radiation at the Redfield site (e.g., Figure 2) are clearly measured over a grassy area, the flux footprint land classification suggests a surface roughness more representative of an area that is 60% grass, 28% shrubs, and 12% trees (Covert 2019).

Finally, comparing the measured ground flux to the simulated ground flux is complicated because the ground flux measurement is made approximately 6 cm beneath the ground surface, whereas Noah-MP computes the ground flux at the bottom of the snowpack as a diagnostic function of the temperature difference between the topmost soil layer and the bottom-most snow layer.

Despite these complications, these additional data are of great value and are used to evaluate the simulation of energy-budget components driving the snow accumulation and ablation in Noah-MP.

2.2 Noah-MP

Noah-MP is a comprehensive LSM that incorporates numerous different physical parameterizations and tuning parameters designed to provide a high degree of flexibility and user control (Niu et al. 2011; Chen et al. 2014). Noah-MP contains an overhead canopy model with parameterizations for snowfall interception and unloading in addition to a two-stream canopy radiation model that modifies the incoming and outgoing radiative fluxes.

In Noah-MP, the snowpack is divided into up to three distinct layers with varying thicknesses, densities, temperatures, and liquid water content (LWC). Heat transfer through the snowpack is simulated using a fully implicit solution to the 1D heat diffusion equation for the combined snow-soil matrix with the snow thermal diffusivity values computed for each snow layer from their respective density and LWC.

Snow layer density increases with time as a function of three parameterized physical processes: (1) destructive metamorphism, (2) overburden, and (3) liquid water infiltration and refreeze. Fresh snow density is determined as an empirical function of the air temperature (Hedstrom and Pomeroy 1998).

In this report, we primarily evaluate the baseline Noah-MP physics configuration used in the NWM. However, we perform a brief analysis of simulation sensitivity to the method used in the model to partition precipitation inputs as rain, snow, or a mix of the two (commonly referred to as the precipitation phase partitioning method). We also present a cursory evaluation of the surface energy budget components of the model with a focus on snow albedo.

2.2.1 Rain/Snow partitioning

The Jordan phase partitioning scheme (OPT_SNF=1) is a reproduction of the parameterization employed as part of the SNTHERM snow model (Jordan 1991). This parametrization allows for both rain and snow to enter the model simultaneously with a snow fraction (f_{snow}) determined as a function of the surface air temperature (T_s):

$$\begin{cases} f_{snow} = 0, T_s > 2.5°\text{C} \\ f_{snow} = 0.6, 2.0 < T_s \leq 2.0°\text{C} \\ f_{snow} = 1 - (-54.623 + 0.2T_s), 0.5 < T_s \leq 2.0°\text{C} \\ f_{snow} = 1., T_s \leq 0.5°\text{C} \end{cases}$$

Interestingly, this function is not actually documented in Jordan (1991), but it appears in the SNTHERM user-guide with an indication that the linear transition from 100-to-60% snow is set arbitrarily.

Noah-MP also provides users the option of establishing the phase partition with temperature thresholds of 2.2°C (OPT_SNF = 2) or 0.0°C (OPT_SNF = 3). With these simplified approaches, the model does not allow for mixed precipitation. Rather, the precipitation type is either 100% rain or 100% snow.

For completeness, we incorporate two additional phase partitioning schemes. In the first, we simply recast the 0°C temperature threshold to a wet-bulb temperature threshold. This partitioning allows for snow to fall at above freezing temperatures if the air is sufficiently dry to support surface air cooling through sublimation.

In the second, we set the frozen precipitation fraction according to output from the High-Resolution Rapid Refresh (HRRR; http://ruc.noaa.gov/hrrr/) model 1-hour forecast. The HRRR is an operational convection-permitting atmospheric model that covers CONUS on a 3 km resolution grid. It is reinitialized every hour with a robust data assimilation cycle to aid in short-term and fine-scale weather forecasting. To implement the frozen fraction of precipitation from the HRRR (hereby referred to as HFFP), the 1-hour forecast HFFP was accessed through the HRRR archive at the University of Utah (Blaylock et al. 2017) and stored locally. The 1-hour forecast was used instead of the model initial analysis since the frozen precipitation fraction was not available in the analysis file. For each NYSM site, if precipitation was recorded at the site, HFFP from the nearest HRRR grid cell containing precipitation was time-interpolated to the geographic coordinates of the site. In rare instances, the distance between the NYSM site and the nearest precipitating grid cell in the HRRR exceeded 50 km. That is, precipitation was measured at the NYSM site but not forecasted by the HRRR. In these instances, the Jordan phase precipitation scheme was used to set the precipitation fraction. These instances accounted for less than 1% of the total wintertime precipitation.

2.2.2 Snow albedo

The snow albedo function from the Biosphere-Atmosphere-Transfer-Scheme (BATS) model (OPT_ALB=1) simulates the decrease in snow albedo for both direct and diffuse radiation in the visible and near infrared bands (NIR) as it metamorphizes in response to temperature and liquid water (Dickenson et al. 1993; Yang et al. 1997). BATS simulates the snow aging process using a non-dimensional snow age (τ_{snow}) that increases in time according to:

$$\Delta\tau_{snow} = \tau_0(r_1 + r_2 + r_3)\Delta t,$$

where τ_0 is a tuning parameter that controls the rate of aging and r_1, r_2, and r_3 represent dry-snow metamorphosis, wet-snow metamorphosis, and metamorphosis from snow impurities, respectively, and Δt is the model timestep. r_1 is given as a function of snow temperature:

$$r_1 = exp\left[r_{1i}\left(\frac{1}{273.16} - \frac{1}{T_{sfc}}\right)\right],$$

where T_{sfc} surface temperature is in Kelvin, and r_{1i} is a tuning constant. r_2 is given as a function of r_1 to represent rapid snow aging as the snow temperature approaches the melting point:

$$r_2 = exp\left[min\left(r_{2i}\left[r_{1i}\left(\frac{1}{273.16} - \frac{1}{T_{sfc}}\right)\right], 0.0\right)\right],$$

where r_{2i} is also a tuning constant. Finally, r_3 is a constant value that represents snow aging due to snow impurities such as dirt or soot. Note that r_3 is not truly representing snow impurities as it has no direct effects on snow albedo, but rather acts as an additional tuning constant that affects the rate of albedo decrease. Note further that there is no explicit adjustment for the aging rate that depends on the presence of liquid water.

The non-dimensional snow age is first used to compute a diffuse albedo (α_d) for the visible and the near infrared (NIR) and is given as

$$\alpha_{vd} = \left(1 - S_v \frac{\tau_{snow}}{1 + \tau_{snow}}\right)\alpha_{v0}$$

and

$$\alpha_{nird} = \left(1 - S_{nir}\frac{\tau_{snow}}{1+\tau_{snow}}\right)\alpha_{nir0},$$

respectively. The α_0 values indicate the "fresh" snow albedo in the visible and NIR, and S is a non-dimensional scaling factor. Note that the default values of 0.2 for S_v and 0.5 for S_{nir} limit the minimum snow albedo to approximately 0.54. Finally, the total snow albedo is adjusted for zenith angles greater than 60°:

$$\alpha = \alpha_d + f\frac{1}{b}\left(\frac{b+1}{1+2bcos(\emptyset)} - 1\right)\alpha_0,$$

where f and b are wavelength-dependent scaling factors that control the impacts of the zenith angle ($\emptyset$).

For zenith angles less than 60°, the total snow albedo is simply the diffuse value. Note that the above equation is applied separately to the visible and NIR albedos where f, b, and α_0 have distinct values for visible and NIR radiation. This zenith angle adjustment represents the increased reflective properties of snow at low incident light conditions, rather than an intrinsic optical property of the snow surface.

A second option for snow albedo available in Noah-MP is the simpler parameterization from the Canadian Land Surface Scheme (CLASS) model (Verseghy et al. 1991). This parameterization treats the snow albedo as a simple exponential decay function that represents snow metamorphosis:

$$\alpha_i = 0.55 + (\alpha_{i-1} - 0.55)e^{-0.01\Delta t/3600},$$

where the subscript "i" indicates the time step index and Δt is the model time step in seconds. Unlike BATS, this parameterization treats snow aging as a uniform process regardless of the meteorological environment the snow surface is exposed to. Further, there is no zenith angle dependence or partitioning into diffuse and direct fractional components. In CLASS, the snow albedo is restored to a fresh albedo of 0.84 once 5 mm of new SWE has replenished the surface.

In this report, we focus solely on the BATS parameterization as it is more physically based and has replaced the CLASS parameterization in the NWM operational setting. Exploratory comparisons of simulations

performed with the BATS (with default parameters) and CLASS parameterizations revealed only minor differences (not shown).

The Noah-MP LSM has a specific input file that contains a collection of tunable parameters that impact various physical parameterizations in the model. This file is named MPTABLE.TBL and is located in the run directory of the model source code. Most parameters that control snow processes in Noah-MP are related to the shortwave energy budget through the BATS snow albedo parameterization. We provide a description of these parameters here to motivate a brief discussion on the snow albedo in the results section (Table 2).

Table 2. Tunable BATS parameters listed in the MPTABLE.TBL file.

Variable	Description	Name	Default
α_{v0}	Fresh snow visible albedo in BATS	BATS_VISNEW	0.95
α_{nir0}	Fresh snow NIR albedo in BATS	BATS_NIRNEW	0.65
b	Scaling parameter for zenith correction in BATS albedo	BATS_COSZ	2.0
f_{vis}	Scaling parameter for zenith correction in BATS albedo	BATS_VIS_DIR	0.4
f_{nir}	Scaling parameter for zenith correction in BATS albedo	BATS_NIR_DIR	0.4
τ_0	Baseline grain-growth parameter for BATS snow aging	TAU0	$1x10^6$
r_{1i}	Grain-growth parameter for dry diffusion in BATS snow aging	GRAIN_GROWTH	5000
r_{2i}	Additional growth due to near-freezing effects in BATS snow aging	EXTRA_GROWTH	10
r_3	Dirt/soot snow aging parameter in BATS albedo	DIRT_SOOT	0.3
S_v	Scaling factor for impacts of non-dimensional snow age in BATS visible albedo	BATS_VIS_AGE	0.2
S_{nir}	Scaling factor for impacts of non-dimensional snow age in BATS NIR albedo	BATS_NIR_AGE	0.5
SWE_{max}	Max new SWE (in mm) required to refresh albedo fully to fresh snow values	SWEMX	1.00

2.3 Noah-MP Single Column Configuration

Distributed snow model output is often evaluated against in situ snow depth or SWE measurements that represent a single point in space. While this can be an effective way to perform a model evaluation over a given region, it is burdened by uncertainty associated with biases in forcing data and land-cover mismatches between the distributed model and the snow gauge. To mitigate this, single-column "point" simulations are a useful tool. In the single-column configuration, the meteorological forcing that drives Noah-MP is supplied directly by the meteorological data measured by a station. Thus, simulated snow processes in Noah-MP can be examined in isolation from uncertainty in the input forcing data. Furthermore, land-cover mismatches can be eliminated by setting the model land-cover classification to that of the exact site location, rather than that of majority land classification within the grid cell that encompasses the station.

In the single-column configuration used here, six of the seven meteorological forcing input variables required to drive the model are taken directly from the NYSM measurements: Temperature, windspeed, relative humidity, downwelling solar radiation, accumulated precipitation, and surface pressure. The downwelling longwave radiation is not measured at the NYSM standard sites and is inferred using the methodology described in section 2.4.1.

In general, the meteorological forcing from the NYSM data is complete with missing data accounting for less than 1.5% of the aggregate 5-minute data network wide. The majority of data outages last for less than 2 hours. In these instances, the missing data are filled in by simply setting the value to the nearest possible time where the data aren't missing. In the few instances where missing data extends beyond 2 hours, the data are filled in using the average taken across all other NYSM stations.

2.3.1 Longwave forcing

We examined four possible methods for determining the downwelling longwave radiative forcing ($LW^{\downarrow}$): (1) assuming black-body radiation according to the 2 m temperature, (2) employing an empirical model for downwelling longwave radiation as described in Izoimon et al. (2003), (3) using the downwelling longwave radiation from the HRRR model analysis

time, and (4) using the downwelling LW radiation from the Analysis of Record for Calibration (AORC) forcing used in the NWM (NOAA 2018).

The first method is the simplest, whereby the longwave forcing is given following the Stephan-Boltzmann relationship for black-body radiation:

$$LW^{\downarrow} = \varepsilon \sigma T^4,$$

where, T is the 2 m air temperature measured by the NYSM, σ is the Stephan-Boltzmann constant $(5.67 \times 10^{-8}\ \mathrm{W\ m^{-2}\ K^{-4}})$, and ε is the apparent emissivity (assumed to be 1 for a blackbody).

The second method uses the clear-sky empirical model described in Izoimon et al. (2003), which estimates $LW^{\downarrow}$ as a function of surface temperature and humidity:

$$LW^{\downarrow} = \left(1 - X_s e^{-Y_s e_v / T}\right) \sigma T^4,$$

where e_v is the vapor-pressure and X_s and Y_s are empirical constants given as 0.35 and 10, respectively.

A key commonality between these two methods is that they both only require input from the NYSM surface data, making them a convenient choice where LW radiation data is unavailable. However, they both ignore the effect of overhead cloud cover which limits their realism. While Izoimon et al. (2003) present a modification of their formula that aims to account for clouds, we posit that estimating overhead cloud cover based on in situ surface observations alone may cause more harm than good in determining downwelling longwave radiation. Additionally, data presented in Izoimon et al. (2003) show slightly *more accurate* estimates of $LW^{\downarrow}$ from their clear-sky model than their all-sky model, which includes clouds.

The remaining two methods used to estimate $LW^{\downarrow}$ both use a dataset that determines $LW^{\downarrow}$ from a sophisticated radiative transfer model applied to vertically variable atmosphere. In the first of these methods, $LW^{\downarrow}$ was pulled from HRRR model simulated data, which uses the Rapid Radiative Transfer Model (RRTMG: Iacono et al. 2000). The HRRR LW radiation is extracted from the grid cell nearest to each NSYM site location, and HRRR hourly output is linearly interpolated to the 5-minute NYSM forcing data.

The final method for estimating the $LW^{\downarrow}$radiation is identical to that of the HRRR forcing, only applied to the AORC forcing used in the NWM.

To assess which method generates the most accurate $LW^{\downarrow}$, the simulated $LW^{\downarrow}$ is compared to the measured $LW^{\downarrow}$ at the SEB sites. At each SEB site, the $LW^{\downarrow}$ is quality controlled and averaged to a 30-minute time interval. For each $LW^{\downarrow}$ method, Noah-MP is run, and the 6 hourly output is compared to 6 hourly mean observed $LW^{\downarrow}$ for each site. This method helps eliminate rapid variability and missing data within the observed downwelling $LW^{\downarrow}$. The results of this analysis are presented in Figure 4. In general, the HRRR and AORC longwave forcing perform the best, generating the highest correlation coefficients and the lowest RMSE (~35 W m^{-2}).

For the two methods based on surface air temperature alone, the results are significantly less accurate. In particular, the blackbody assumption systematically overestimates $LW^{\downarrow}$, and the Izoimon et al. (2003) method systematically underestimates it. The blackbody assumption could be improved by simply treating the air as a gray body with an emissivity less than 1. Notably, simulated $LW^{\downarrow}$ is underestimated for every compared value in the Izoimon et al. (2003) method. While incorporating an adjustment for clouds would likely alleviate this underestimate, it would not entirely correct the issue because several of the observations occurred under cloud-free skies. Rather, we speculate choosing X_s and Y_s parameters more suited to the NEUS region would yield better results. Based on this analysis, we chose to use $LW^{\downarrow}$ forcing from the HRRR analysis cycle interpolated to the 5-minute NYSM forcing data in all of our subsequent analyses.

2.3.2 Vegetation type in the point configuration

One of Noah-MP's defining characteristics is the inclusion of a sophisticated forest canopy layer based largely on Hedstrom and Pomeroy (1998). This layer has substantial impacts on SEB and water mass balance of the simulated snowpack by attenuating the shortwave radiation reaching the ground, intercepting and holding snow within the canopy where it is subject to increased sublimation, modulating the near surface wind, and changing the overall surface albedo, thereby lessening the impact of snow albedo on the SEB. Critically, while 112 out of 126 sites are classified as either deciduous or mixed forest in the NWM, the majority of NYSM sites are located in clearings, suggesting that direct comparisons

between NYSM measured snow and NWM simulated snow are likely biased (Figure 5). Furthermore, at the few NYSM locations that are located either beneath or in very close proximity to trees, the instrumentation is situated below the canopy top, and therefore the forcing data measured by the NYSM are already registering the impacts of the overhead canopy. To avoid these issues, we choose to represent the land cover as grassland for all sites.

Figure 4. Scatter plots showing observed downwelling longwave radiation and longwave radiation prescribed using various methods. The black dashed line is the one-to-one line. The RMSE and linear regression slope and r2 values are indicated for each method.

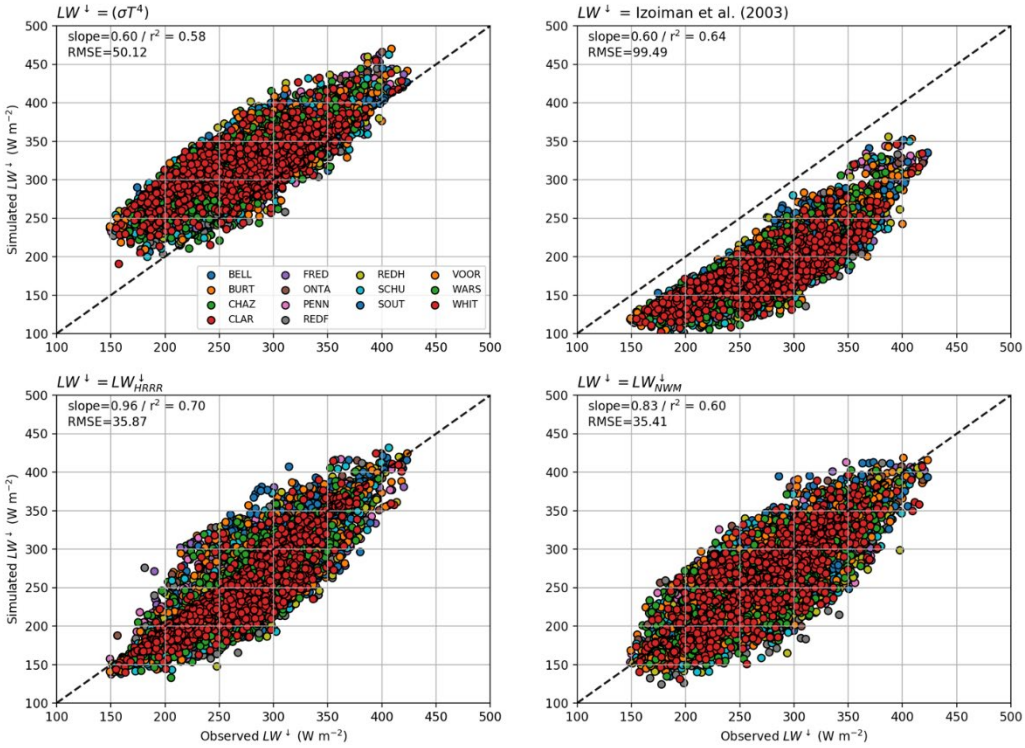

We acknowledge that this choice may have a negative impact on the turbulent fluxes at sites in close proximity to forest edges as these fluxes are more driven by the broader area surrounding the NYSM rather than the specific site location itself. However, this ensures that solar radiation and precipitation are not artificially reduced.

Figure 5. Photographs of three exemplary sites within the NYSM that are classified as forested in the NWM. Site locations are marked on satellite images from Google Earth.

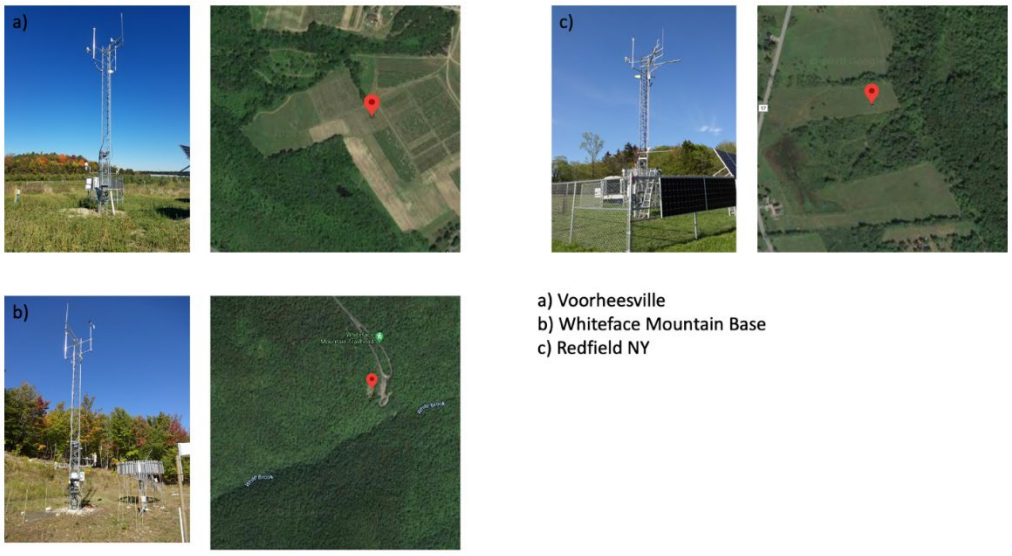

a) Voorheesville
b) Whiteface Mountain Base
c) Redfield NY

3 Results

3.1 Overview

Since snow depth and SWE are bounded variables (i.e., they have a physical lower limit of 0.0 m), it is challenging to interpret standard quantitative metrics such as RMSE and percent bias. As a result, we chose to perform the evaluation of the standard network by comparing simulated and observed snow depth time series at individual NYSM sites and by using the following three metrics to evaluate the model geographically: (1) Maximum snow depth, (2) mean snow depth, and (3) number of days with snow cover. In computing the number of days with snow cover, a data point is considered snow free when the snow depth is less than 1 cm. In all quantitative comparisons, the smoothed snow depth time series is resampled to the model output time interval through averaging.

Figure 6 provides a spatial summary of these results for the 2019–20 winter season, defined here as October 1–May 31. This year was chosen instead of the 2018–19 season because there were more available snow depth observations. However, the results are broadly similar between both winters.

Noah-MP performance with respect to snow is variable across the NYSM sites; however, on average, the model produces deeper and more persistent snow covers at a majority of NYSM locations.

For instance, Noah-MP averages 13 days of additional snow cover for the 2019–20 winter season, with an average maximum snow depth approximately 20 cm deeper than observed. In general, the model performs better with respect to snow at NYSM locations with less persistent snow cover. We suspect that this is likely due to the fact that model errors do not have as great an opportunity to accumulate at sites with less snow than they do at the snowier sites.

The snowiest sites, particularly the ones situated in the Adirondack Mountains and Tug Hill Plateau that make up the Northern Plateau climate division, have differences in maximum snow depth exceeding 0.5 m and melt out dates greater than 3 weeks later than observed. This is exemplified in Figure 8, which shows selected time series of simulated and observed snow depth for the 2019–20 winter season. In each instance, the

simulated snow is generally deeper and persists longer into the spring than observed. A comparison between the simulated and observed top-layer soil temperature reinforces this, as the observed top-layer soil temperature begins to warm earlier than simulated at all locations corresponding to the difference in the snow melt out date (Figure 7).

Figure 6. 2019–20 season observed number of days with snow cover, mean snow depth, and maximum snow depth (left column). Baseline observed difference in days with snow cover, mean snow, and maximum snow depth (Right column). Depth is in meters.

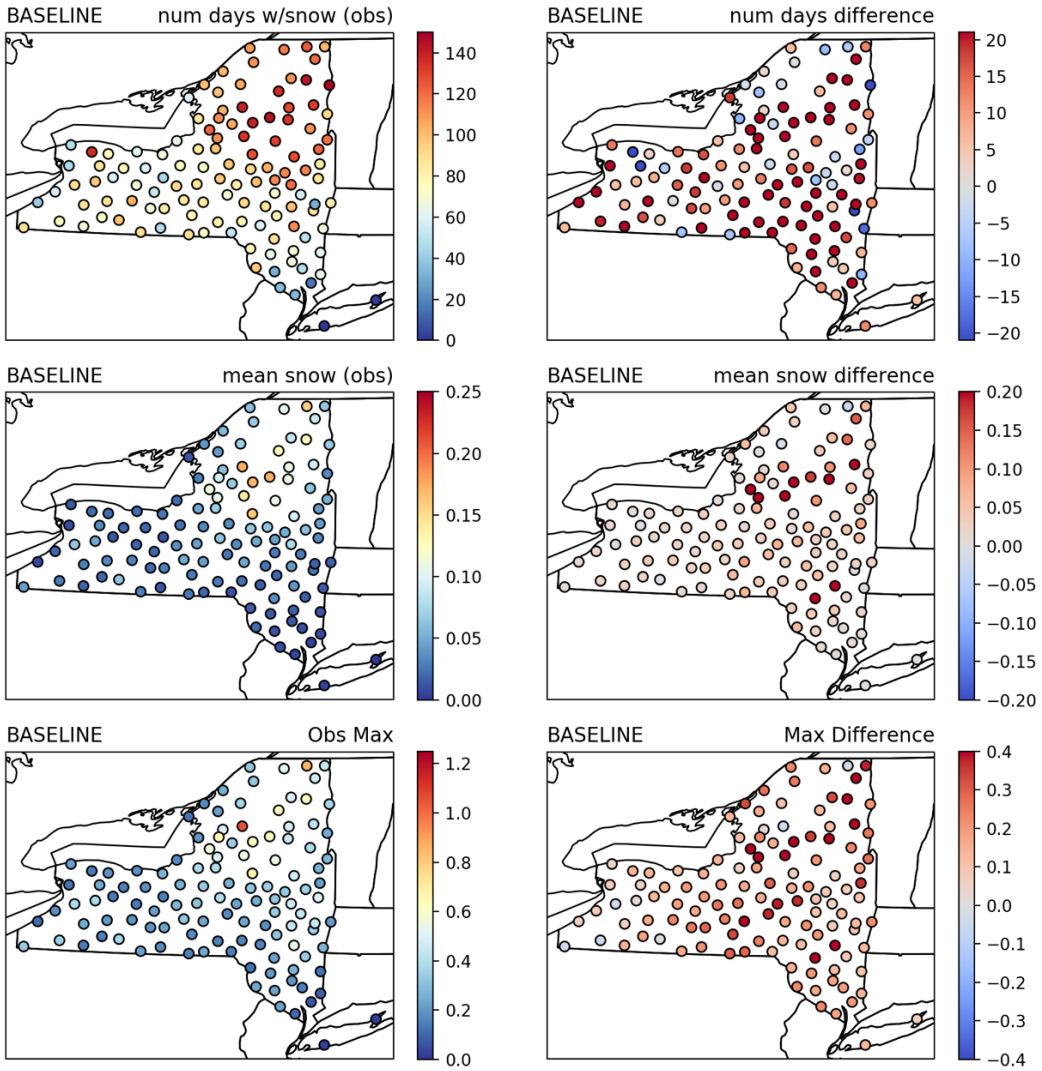

Figure 7. Time series of simulated and observed snow depth at four sites within the NYSM for the 2019–20 winter season. Site locations are indicated in geographic insets. Simulated snow and soil temperature are shaded. Observed soil temperature is overlaid as color-filled markers.

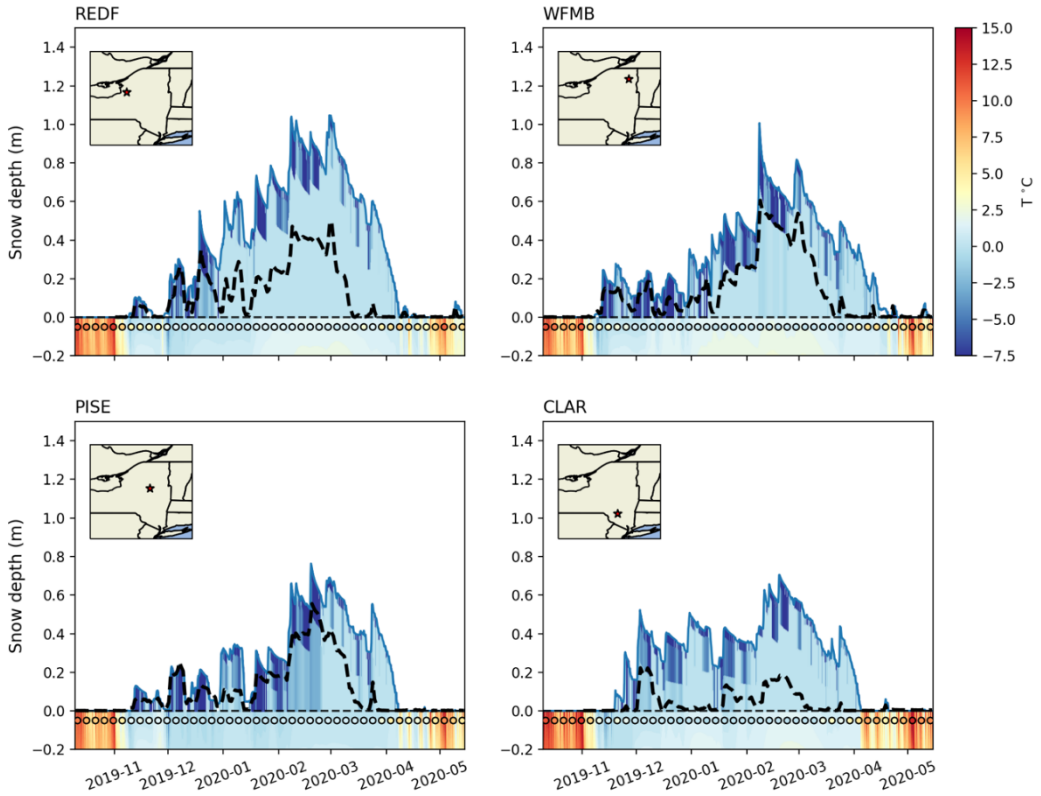

3.2 Sensitivity to Precipitation Partitioning and Comparison against Snow Sites

Precipitation phase partitioning is a significant source of error and uncertainty in hydrologic models (Harder and Pomeroy 2014). Here we investigate the impact of precipitation phase partitioning in the NEUS and aim to determine which partitioning method is most accurate. This analysis takes advantage of the multi-parameterization options in Noah-MP and reveals that the phase partitioning method has a dominant impact on simulated snow in the NEUS. In particular, reducing the threshold rain/snow temperature to 0°C systematically improves the results at nearly every site in the domain (e.g., Figure 8). For instance, this change results in a decrease in the mean difference in maximum snow depth from 20 cm to 10 cm. It also results in mean improvement in snow cover duration, decreasing the overestimate in the number of snow days from 14 to 1. The change from the baseline to a temperature threshold of 2.2°C has little overall effect, in part because this modification does not have a

substantial impact on the diagnosed precipitation phase relative to the Jordan (1991) parameterization.

Figure 8. Simulated-observed maximum snow depth difference (meters) for each precipitation phase partitioning method for the 2019–20 winter season.

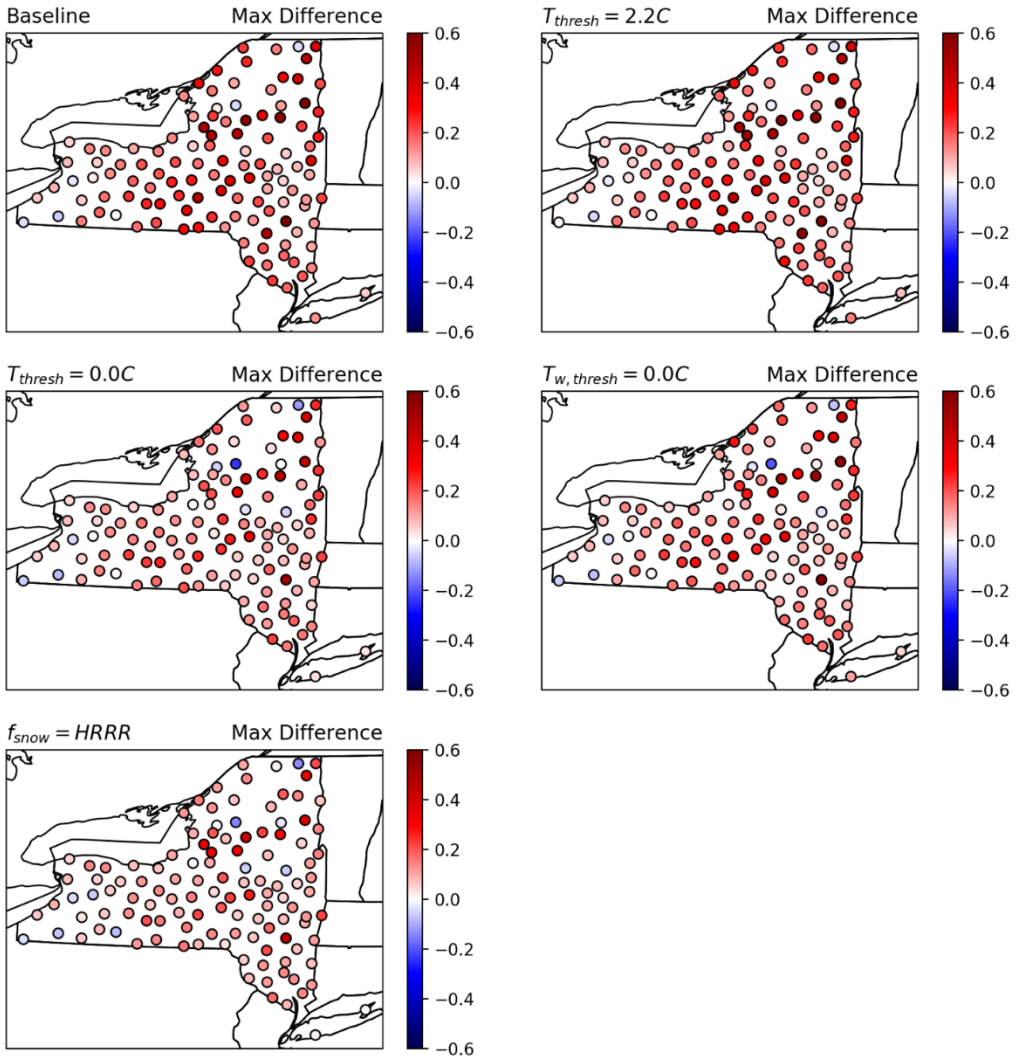

These results support the conclusions of Jennings et al. (2018), which indicate that the threshold temperature delineating rain and snow across the eastern US is near to 0°C. Setting the phase threshold to a Tw=0°C yields a result in between the T=0°C and Baseline simulations. While setting the precipitation phase from the HFFP produces the most accurate snow depth with the lowest mean difference between the model and observations, the improvement relative to the T=0°C simulation is variable across the network.

A more robust analysis of the impacts of precipitation phase partitioning on simulated snow is performed against the continuous SWE observations from the snow network. We first compare simulated and observed time series of SWE at each individual site with each precipitation phase partitioning method for the 2019–20 winter season (Figure 9).

Figure 9. Simulated and observed SWE for each site within the NYSM snow network for the 2019–20 winter season. Observed SWE is color filled, and simulated SWE for each precipitation phase partitioning method is indicated in the legend. Sit locations are shown in the geographic insets. Note a prolonged data outage at the Raquette Lake site that persists from December through late January.

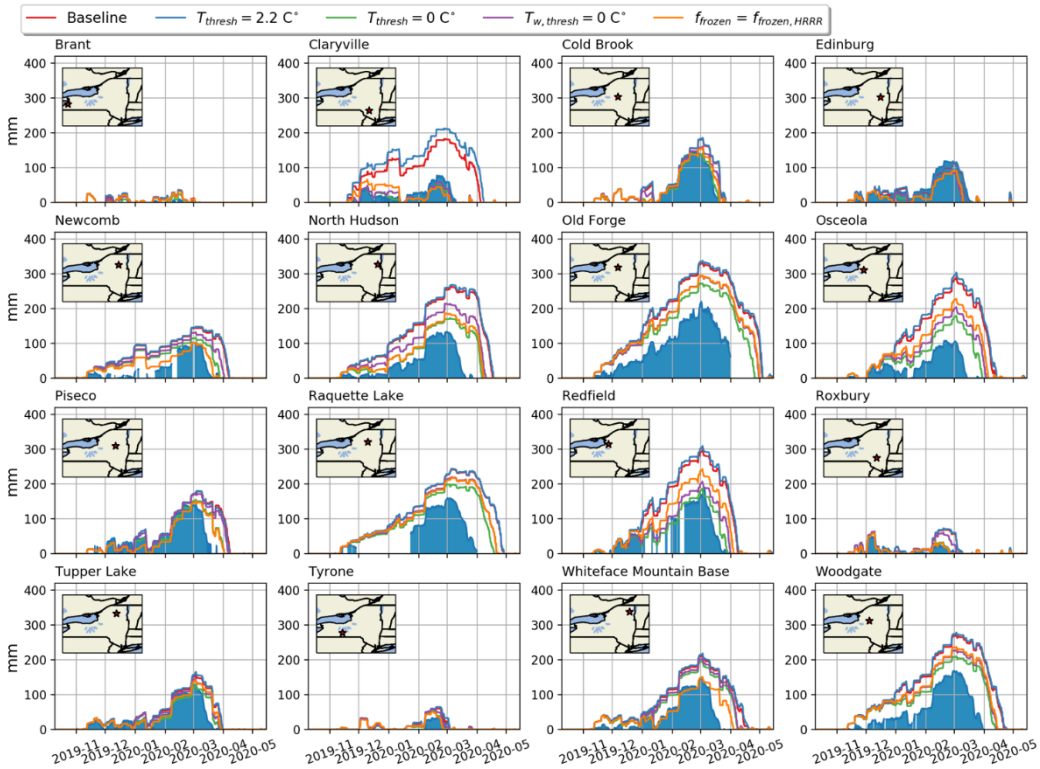

While site performance is variable, a consistent pattern emerges across a majority of sites that shows a large overestimate in SWE in the baseline simulation that is substantially mitigated when the rain/snow partitioning is replaced with a 0°C threshold or with the HFFP. In particular, Noah-MP overestimates peak SWE by ~300% at Claryville in the Catskill Mountains Baseline configuration (Figure 9). This overestimate is replaced with a small underestimate when using the 0°C threshold. Other sites show similar improvements where the 0°C threshold reduces or entirely resolves the SWE overestimate in the baseline simulation. Furthermore, sites where Noah-MP performance is relatively good in the Baseline simulation

are not negatively impacted by a change in precipitation phase partitioning method (e.g., the Edinburg site in the southern Adirondacks).

We expand upon this analysis using the multi-metric methodology described in Rhodes et al. (2018). In this methodology, the season is broken into two time periods separated by the date of maximum SWE. The accumulation period is defined by the time period prior to the date of maximum SWE where SWE depth is greater than 10% of its maximum value. The melt season is defined by the time period after the date of maximum SWE where SWE depth is greater than 10% of its maximum value. From these definitions, a mean accumulation rate and ablation rate can be determined for each site. This analysis is presented in Figure 10 and Figure 11, which show histograms of simulated and observed differences for each precipitation phase partitioning method. These histograms comprise all snow sites without continuous data outages that persist for longer than two days for both the 2018–19 and 2019–20 winter seasons.

This analysis shows significant improvement in the melt out date, maximum SWE, and mean accumulation rate when the Baseline Jordan phase partitioning method is replaced with the 0°C threshold or the HFFP. Further, while the length of the melt season is also improved, the mean melt rate is largely unaffected by the phase partitioning method.

While clear improvements in the simulated SWE are achieved by modifying the phase partitioning method, a more direct evaluation of the phase partitioning is achieved by estimating an observed season accumulated total snowfall through a summation of the measured time-rate-of-change of SWE for all positive increments. Note that in the observations, rain that refreezes into the snowpack will be counted as SWE, making this an imperfect measure of snowfall. This analysis allows for an evaluation of the precipitation phase partitioning in isolation of errors caused by snow ablation. Prior to analysis, the data at each site were carefully examined for any additional artifacts and for general consistency with the snow depth measurements. Periods of missing data that spanned fewer than 2 days during the snow season were filled by linear interpolation. Sites with substantial amounts of missing data or clear artifacts were discarded from analysis.

Figure 10. Histograms of the (model-observed) differences in melt out date, accumulation season length, and melt season length. Precipitation phase partitioning method and mean bias (days) are indicated in each panel.

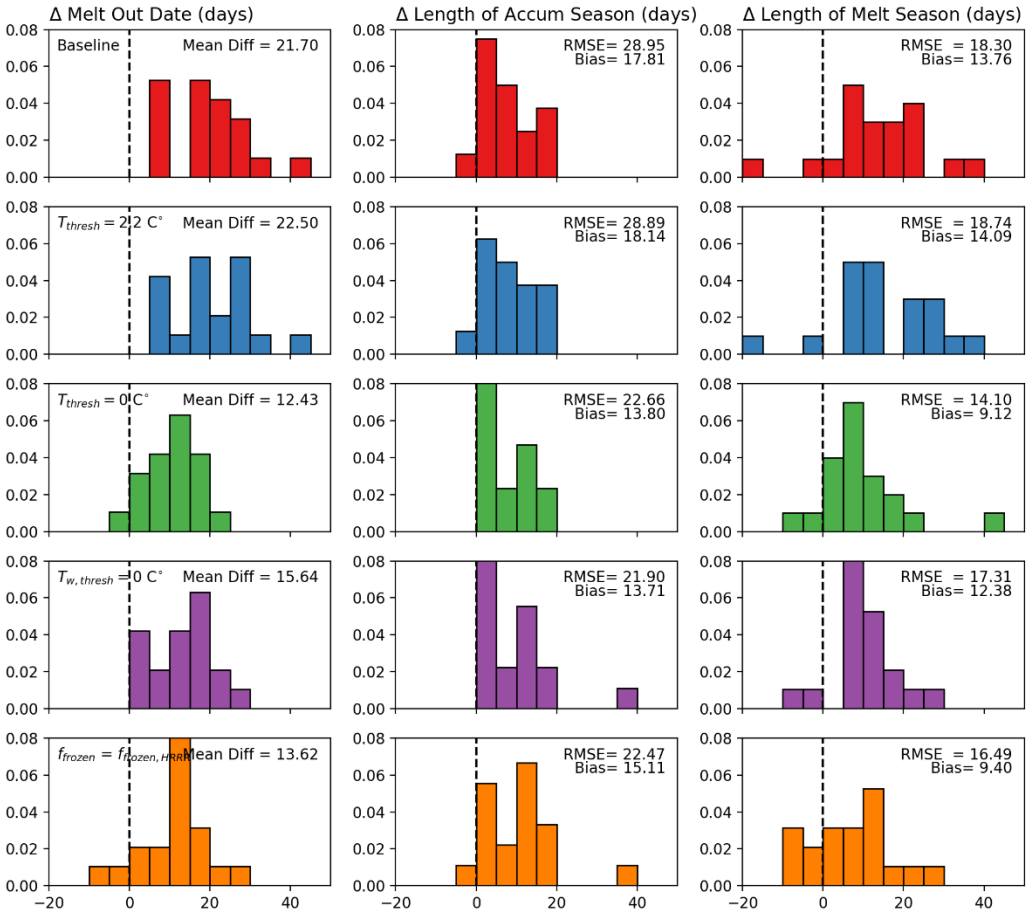

Figure 11. Histograms of the (model-observed) differences in accumulation rate, melt rate, and maximum SWE.

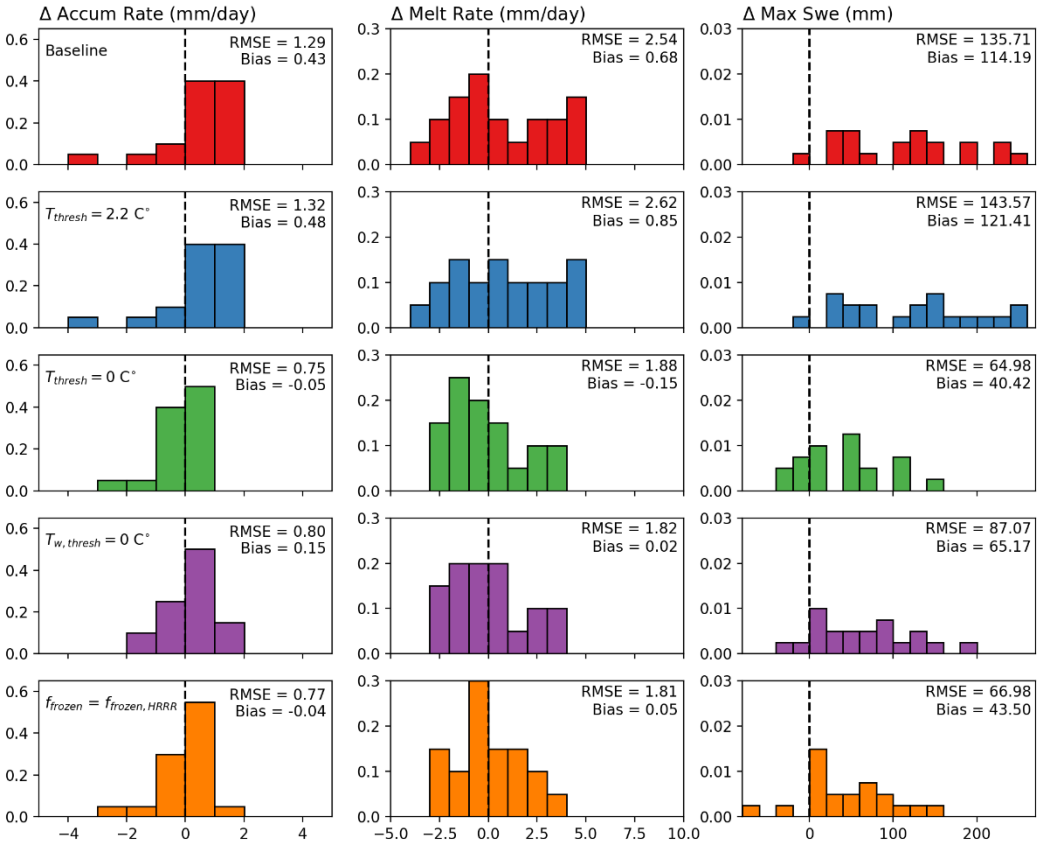

The SWE data are first smoothed using a daily running mean to remove high-frequency noise during quiescent periods that can be incorrectly counted as snowfall. An example of this methodology is presented in Figure 12, which shows the accumulated SWE at the Whiteface Mountain Base (WFMB) site for the 2019–20 winter season for both the smoothed and unsmoothed data. Note that in this example, the smoothing reduces the total accumulated SWE by approximately 55 mm.

This methodology is applied to all sites, and histograms of the difference between simulated and estimated season-accumulated snowfall for each precipitation phase partitioning method are compared (Figure 13). This analysis reveals that the HFFP partitioning method is most accurate and further shows the overestimate in snowfall for the Baseline method. These results are further summarized in Table 3 using root mean square error (RMSE), absolute bias, and r^2.

Figure 12. Example, showing the impact of smoothing on the total accumulated SWE in comparison to the model-simulated SWE accumulation. Top: Time series of raw and smoothed SWE. Bottom: Measured and simulated total accumulated SWE comparing the difference between the raw and smoothed SWE time series.

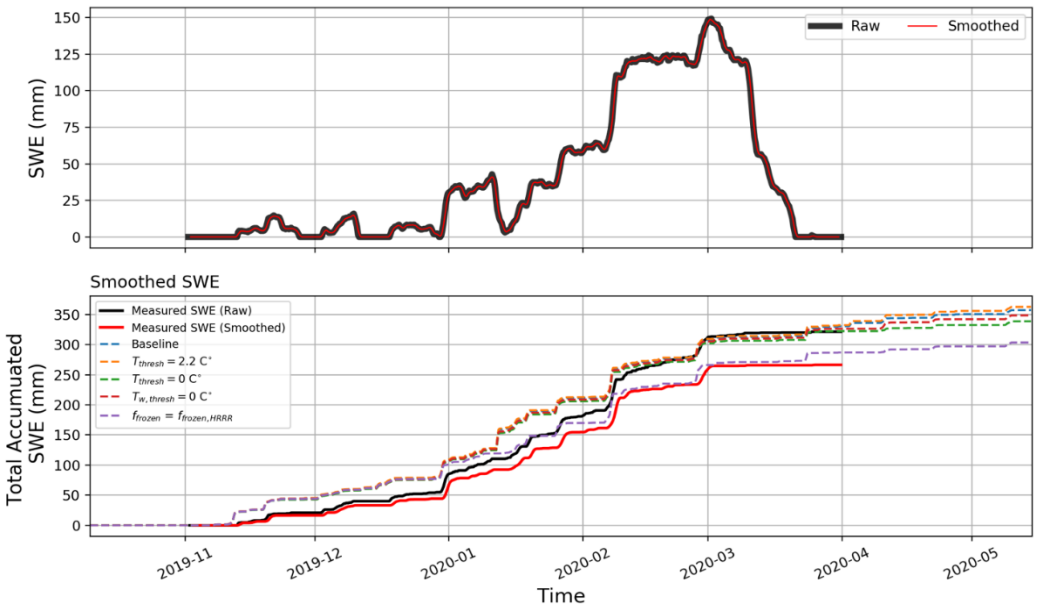

Based on the evaluation of Noah-MP against the NYSM snow network, we concluded that the HFFP provides the most accurate precipitation phase forcing for the point simulations. In particular, this method substantially improved the simulated SWE, mean snowfall accumulation rate, and melt out date. Further, the HFFP phase partitioning showed the best agreement with the estimated cumulative snowfall with an RMSE of 61 mm and a bias of 2 mm. This result is consistent with a broader finding that showed network-wide improvement in maximum snow depth when using the HFFP rather than the Baseline method (Figure 8).

Table 3. Quantitative comparison between simulated and observed season accumulated snow at all snow sites using smoothed SWE time series

Simulation	RMSE (mm)	Bias (mm)	r^2
Baseline	135	112	0.60
T2.2	146	122	0.60
Tzero	84	−11	0.5
Twet	69.5	36.8	0.49
HFFP	61	2	0.44

Figure 13. Histogram showing differences between simulated and observed total accumulated SWE (mm) using the smoothed SWE time series for each precipitation phase partitioning method.

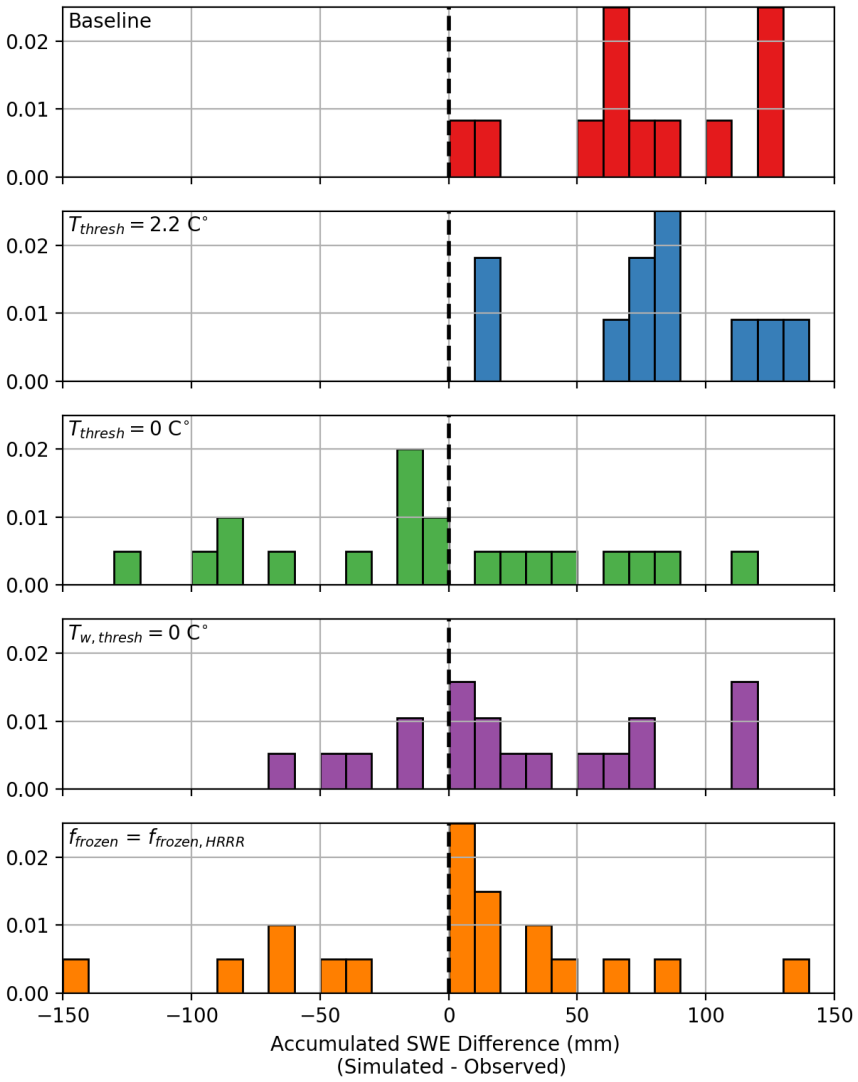

3.3 Role of NEUS regional climate

Climatological conditions may help explain the high regional sensitivity to precipitation phase partitioning in the NEUS. To explore this, we first compare the percent differences in total accumulated simulated snow water equivalent (mm) relative to the Jordan precipitation phase partitioning method at the end of each experimental simulation to identify spatial patterns in this sensitivity. Figure 14 shows that using the 0°C threshold or HFFP type can reduce the snowfall by more than 50% at some sites, particularly in the southern and eastern part of the state in the lower elevation bands. The HFFP reveals an even greater spatial contrast between the northwest and southeast. Further analysis reveals that this

may be due to the closer proximity to the coast where the temperatures are more likely to fall within the precipitation phase transition range during precipitation events (not shown).

Figure 14. Percent snowfall reduction, relative to the Jordan scheme, at each NYSM site for the 2019–20 season by modifying the precipitation phase partitioning scheme.

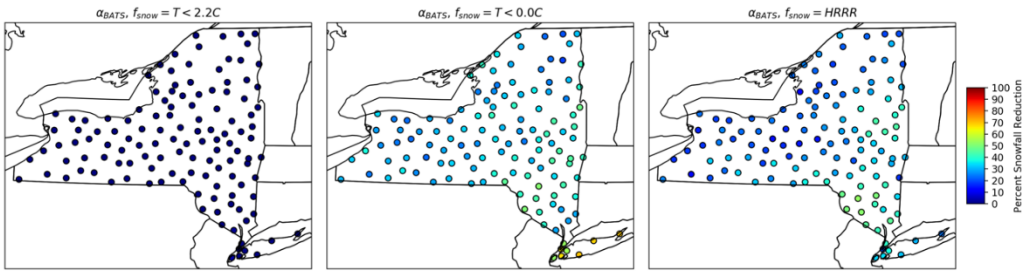

The surface precipitation phase is determined by the kinematic and thermodynamic properties of the local atmospheric column, as well as the microphysical properties of the precipitation falling throughout the column. Under typical atmospheric stratification, where temperature decreases with height, the warmest temperature within the lower troposphere is the surface temperature. Under these conditions, hydrometeors are likely to remain at least partially frozen for surface temperatures just slightly above 0°C. In contrast, when warm air overruns colder air at the surface, as is common during mid-latitude cyclones, an inverted thermodynamic profile develops that allows for above-freezing air to persist from the surface to 1–2 km above the surface and at higher altitudes, despite the fact that the surface temperature is near or just above 0°C.

To investigate the role of atypical atmospheric thermal stratification, we plot a composite of an atmospheric Skew-T log-P diagram from measurements taken from radiosondes released from the National Weather Service in Albany, New York, for the 20 events where the HRRR precipitation phase differs most significantly from the baseline Jordan phase partitioning at the nearby NYSM Voorheesville site (Figure 15). Voorheesville was chosen as it is the site nearest to the National Weather Service at Albany. Events are determined from the daily difference in accumulated snowfall between the two parameterizations. This analysis provides some insight into the mean vertical temperature profile that represents the precipitation events that are most affected by the precipitation phase partitioning method.

Figure 15. Composite Skew-T Log-p diagram for Albany, New York, for the 20 events where precipitation phase most impacted the results. Thick Lines = average, thin lines represent each individual event.

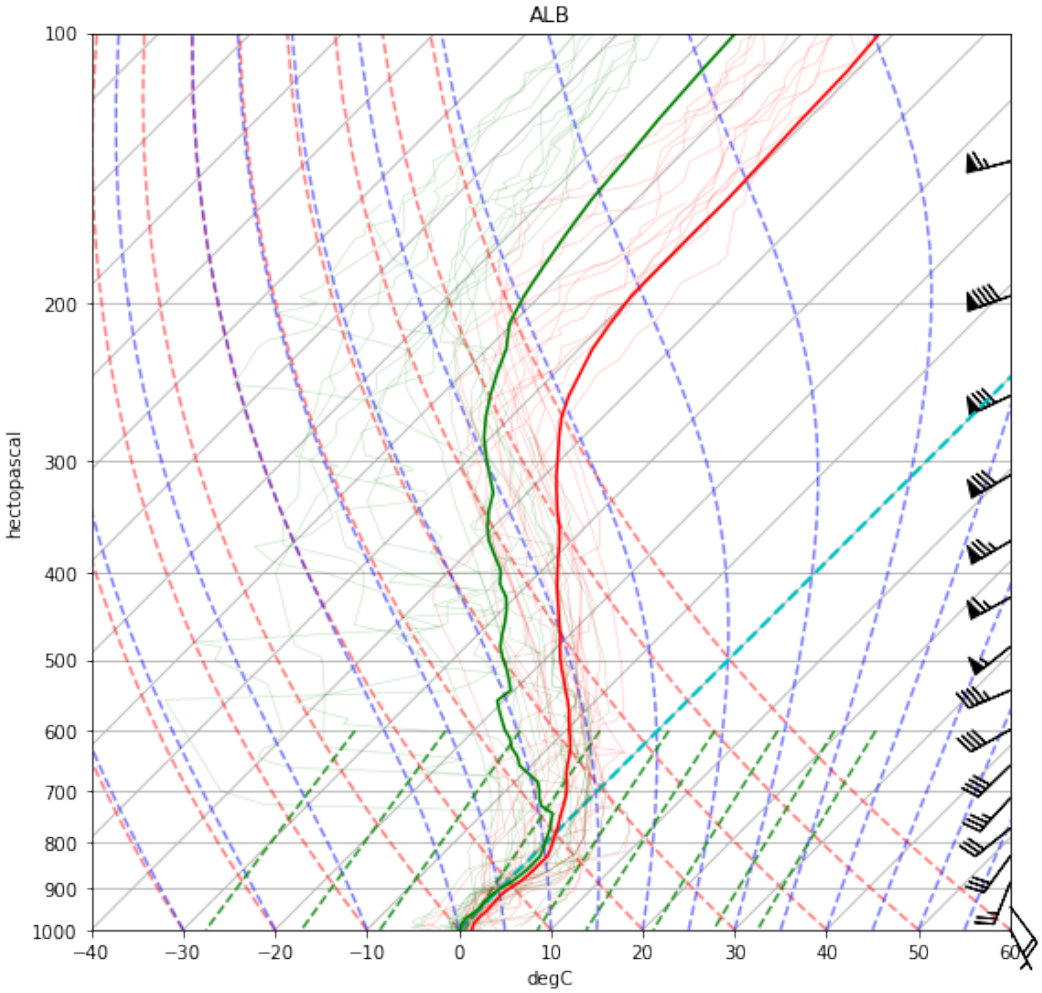

We find that the composite sounding has a veered wind profile (i.e., clockwise directional turning) indicative of warm air advection and a nearly isothermal temperature profile with a mean temperature of approximately 0.25°C between the surface and 800 hPa level, suggestive of a layer experiencing diabatic cooling from melting snow. Note that the 800 mb layer exceeds the highest elevation in the NEUS, indicating that the precipitation type is likely to be at least partially liquid even at the highest terrain in the NEUS.

This analysis helps explain the high degree of sensitivity the NEUS has to the precipitation phase partitioning and highlights challenges in approximating precipitation phase partitioning from surface conditions alone. This is perhaps best exemplified by the fact that the precipitation

phase determined from an atmospheric model outperformed all surface conditions–based methods. Further, this analysis points to a larger challenge in downscaling relatively coarse numerical weather prediction data onto a higher resolution terrain dataset, which requires a shift away from physically based atmospheric models toward simpler precipitation phase partitioning methods.

3.4 Flux Comparison

As a final analysis in this report, we leverage the surface energy budget data within the NYSM to understand and improve how energy transfer between the snow cover and atmosphere is simulated in Noah-MP. To compare the Noah-MP output against the flux data, the simulations are rerun with output generated every 30 minutes to match the 30-minute average quality-controlled flux data produced by the NYSM. Note that in the following analysis, the net radiative flux and the ground flux are oriented such that positive values indicate downward heat fluxes, whereas the turbulent fluxes are oriented such that positive values represent upward heat fluxes.

We first evaluate model performance by comparing the mean diurnal cycle of the SEB components averaged over all available SEB sites between October 2019 and April 2020 (Figure 16).

In general, the model performs best at night; however, it appears to substantially underestimate the surface temperature. There are larger differences between the model and observations during the daytime. In particular, differences between the simulated and observed net radiation, sensible heat flux, and ground flux amount to a net energy flux difference of approximately −35 W m^{-2} in the snowpack, indicating that, taken together, the snowpack simulated by Noah-MP has less energy available to melt snow as observed. Further breaking the net radiation into shortwave and longwave flux components reveals that this difference is caused by underestimates in both the simulated upwelling longwave radiation flux due to a lower snow skin temperature and the absorbed solar radiation caused by differences in surface albedo (not shown).

Figure 16. Diurnal cycle of the SEB components over snow cover. Time is in UTC. Averaged over all times and stations during the 2019–20 winter season.

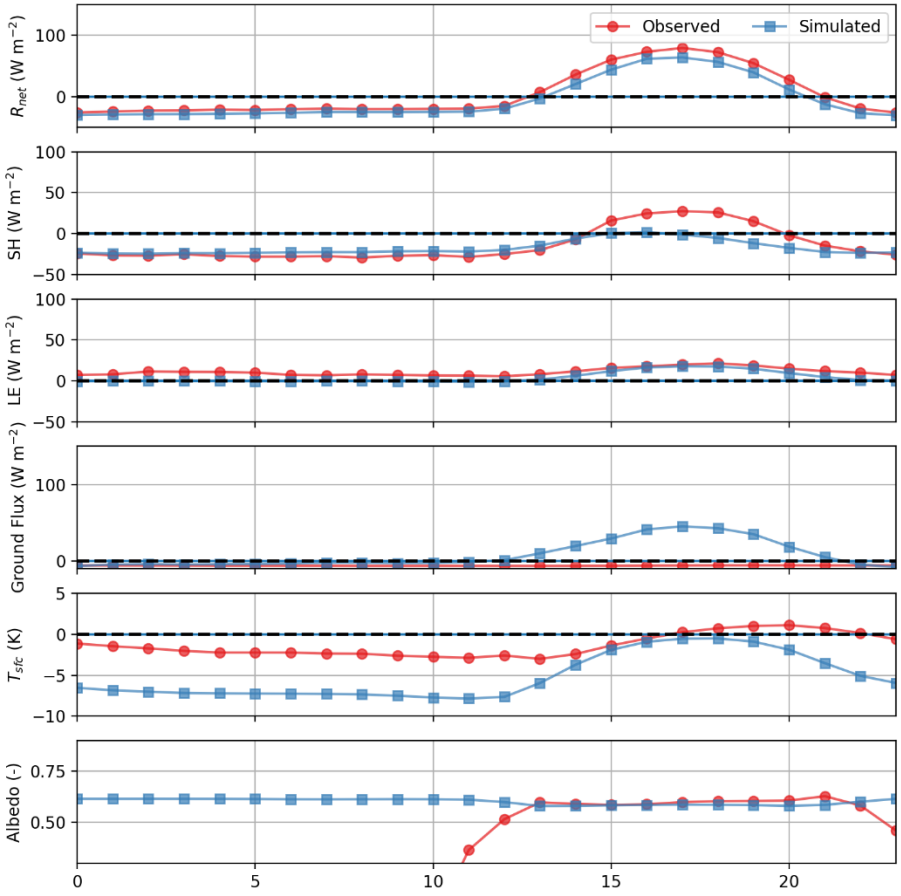

To understand how these differences vary throughout the winter season, the difference between the simulated and observed SEB components over snow are computed for each month of the 2019–20 winter season (Figure 17). November and April are excluded from this analysis due to an insufficient number of samples with both simulated and observed snow cover.

This analysis reveals that the largest biases in the model fluxes occur during March. In particular, the simulated net radiative flux is most underestimated during this time. Further, this underestimate appears to be associated with an overestimate in surface albedo, indicating that the model is reflecting more solar radiation than observed. Additionally, while the ground flux is overestimated during all months, this overestimate is largest during March.

Figure 17. Diurnal cycle of simulated minus observed SEB component differences for the months November 2019 through March 2020. Averaged over all flux stations.

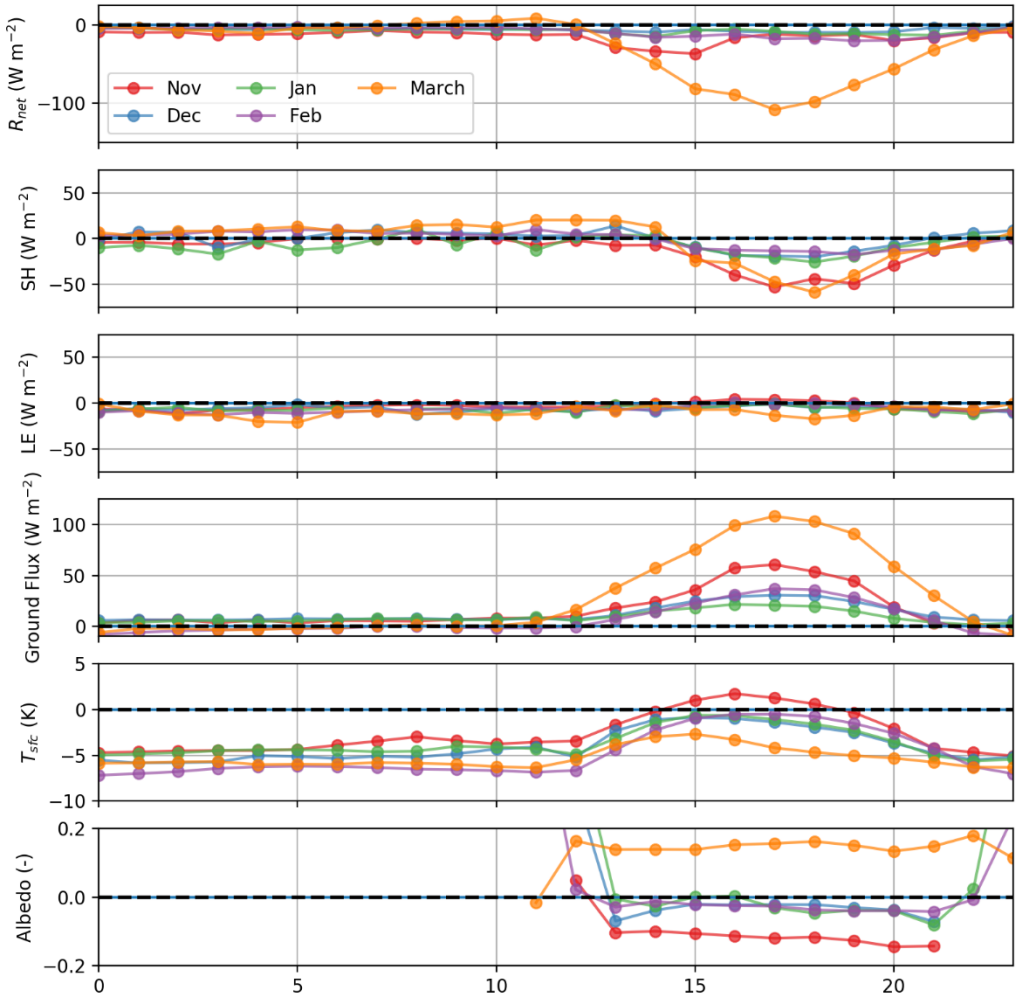

To illustrate evolution of the SEB components in connection with the observed snow surface, we briefly perform a more in-depth examination of a 13-day period spanning February 28–March 12, 2020, at the Redfield site (Figure 18). This period was chosen because it spans a time period where the measured snow depth decreased from approximately 55 cm to 5 cm in response to a series of rain-on-snow events that occurred on March 2, March 6, and March 10. At selected times throughout this period, automated site photography is used to qualitatively assess the snowpack (Figure 19).

Figure 18. Simulated and observed SEB components for the Redfield NYSM site between February 28 and March 12, 2020. The markers on the albedo panel indicate daily median albedo. Simulated and observed snow depth are shown on the bottom-most panel. The star markers on the bottom panel show where automated site photographs are used to visually inspect the site.

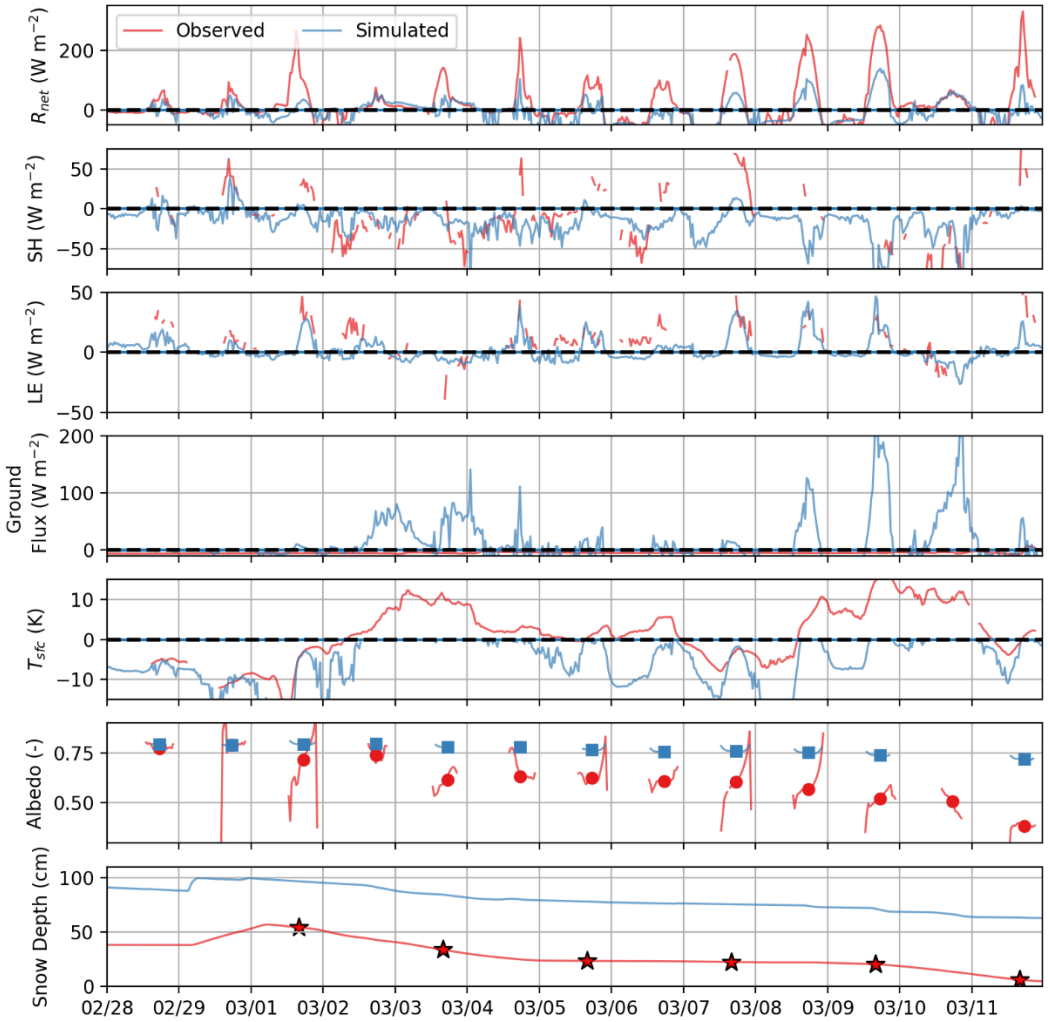

The simulated and observed net radiation generally agree during nighttime and under cloudy conditions, but the model substantially underestimates net radiation on sunny days (Figure 19). Interestingly, the measured surface temperature exceeded 0°C on the dates with rain-on-snow events. We speculate this may be measurement error due to the fact that the downward pointing radiometer is likely incorporating the temperature of the exposed ground and vegetation, in addition to the tower infrastructure, into its measurement.

Figure 19. Automated site photographs from the Redfield site corresponding to the markers in Figure 19. Each image is taken at 11:55 a.m. local time. The measured daily median albedo is shown in each panel.

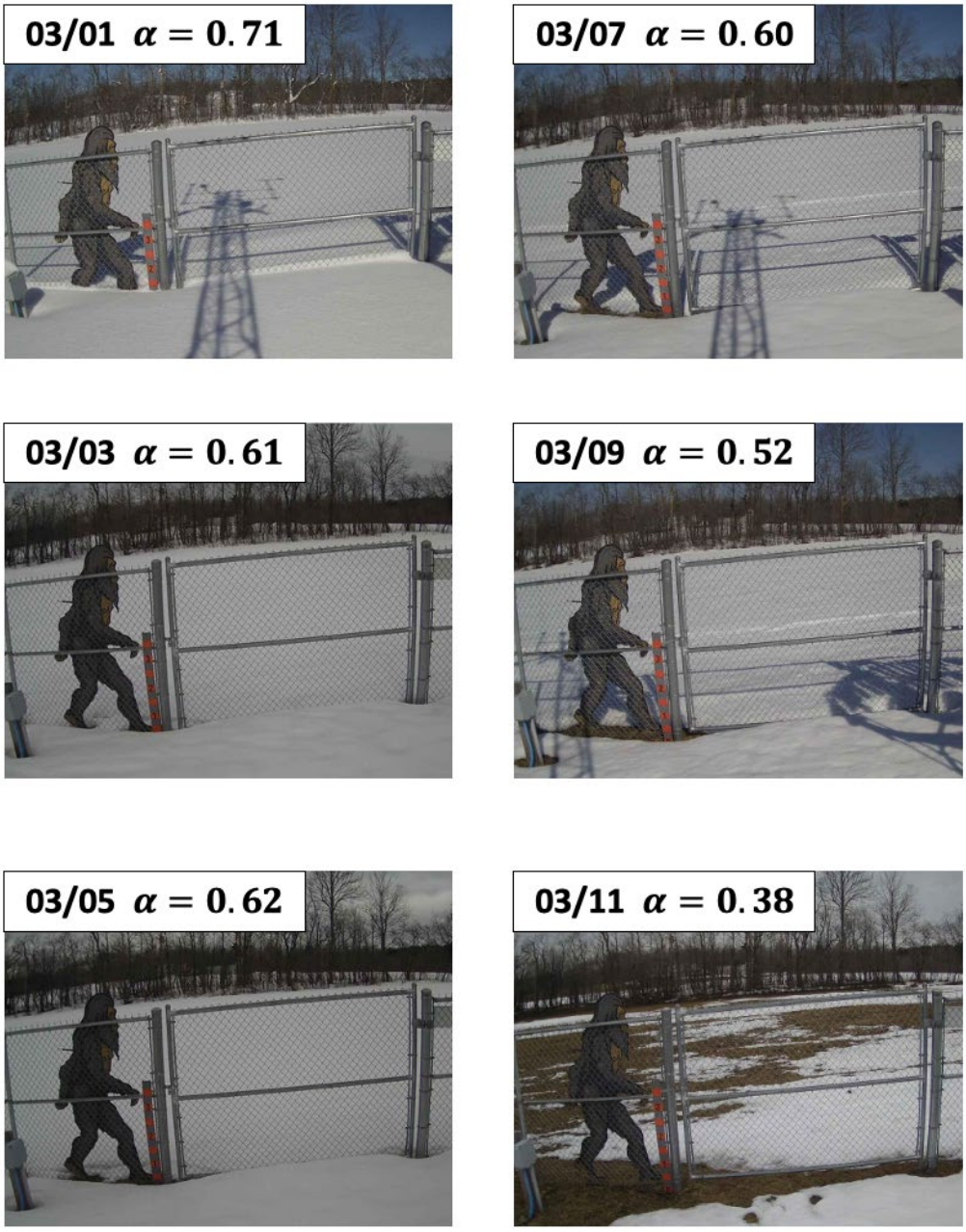

There are substantial differences between the simulated and observed ground flux. In particular, the simulated ground flux often exceeds 100 W m^{-2} during the daytime, whereas the observed ground flux typically remains constant and slightly negative, indicating a constant and almost negligible upward heat flux into the snowpack. It is difficult to robustly compare the measured and simulated ground fluxes. For instance, the

measured ground flux is determined using input from a sensor that is approximately 6 cm beneath the surface and is estimated using a semi-empirical formula relating the heat flux to the sensor output (Covert 2019). In contrast, Noah-MP computes the ground flux as a diagnostic variable proportional to the temperature difference between the bottom-most snow layer and topmost soil layer taken over the bottom snow layer depth (Niu et al. 2011).

The difference in daily net solar radiation can be partially explained by the difference between the simulated and observed surface albedo. At the beginning of the time period, the simulated albedo is close to the observed. These values first start to diverge after the first rain-on-snow event that occurred between approximately 0300–0800 UTC on March 3. A comparison of site photographs taken on March 1 and March 3 reveals a qualitative change from a fresh snow surface to one that appears more compacted (Figure 19).

The observed daily median albedo then remains somewhat constant in time at approximately 0.6 until March 8, after which a second rain-on-snow event further decreases the albedo. Notably, the simulated albedo does not decrease accordingly with either rain-on-snow event. A third rain-on-snow event occurred on March 10, which completely melted the snow in places, further reducing the measured albedo to less than 0.4, indicative of mixed snow/ground cover. At this time the observed albedo is not comparable to the model since the model snow depth would indicate 100% snow cover.

This analysis exposes two important considerations: (1) the BATS snow albedo parameterization appears to underestimate the rate of snow aging in this region, in particular the decreases in albedo that occur in response to rain-on-snow events; and (2) the impacts of underestimating the albedo are most detrimental to the snow simulation during March when the sun angle is high. These results can partially explain why the simulated melt out date is later than the observed melt out date, even after improving the rain/snow partitioning method.

In summary, the SEB analysis reveals apparent shortcomings in the simulated snow albedo and ground flux, which act to reduce the amount of energy available for snowmelt throughout the winter season in Noah-MP, contributing to the mean overestimate in peak snow depth and SWE as

well as a prolonged melt season. Future efforts evaluating the simulated SEB components over using the NYSM will focus on better understanding the role of the snow albedo ground flux parameterizations in driving model biases in snow.

4 Conclusions

In this report, we demonstrated how the NYSM is used to understand sources of error in simulated snow within the Noah-MP LSM configured as in the NWM over NEUS. This analysis was performed by using 5-minute interval meteorological forcing from the NYSM measurements to drive the Noah-MP LSM for each NYSM site. The models were evaluated against acoustic snow depth measurements installed at every NYSM site and gamma ray SWE sensor measurements installed at a selection of enhanced sites embedded within the NYSM. Further model evaluation of the SEB components was performed using the SEB network. The point simulation methodology in conjunction with the advanced observational datasets available from the NYSM aided in isolating errors caused by specific model processes and parameterizations, thereby reducing the influence of compensating errors on the interpretation of the results. The key conclusions of this work are summarized below:

- Data collected from the flux stations revealed that using downwelling LW radiation from either the HRRR or the AORC compared better to the observed downwelling LW fluxes than simpler temperature-based formulas that are often used in absence of more sophisticated LW forcing data.
- The default precipitation-phase partitioning scheme used in the NWM substantially overestimates the total annual snowfall at most sites, leading to systematic high-biases in snow depth and SWE throughout the region. Lowering the temperature-based threshold to 0°C significantly improves the results. Additional sensitivity tests show that determining the precipitation phase from HRRR model produces the most accurate results in aggregate.
- The high degree of sensitivity to the precipitation phase partitioning is spatially variable over New York State, with the greatest sensitivity in the southeast part of the state, where over 30% of wintertime precipitation falls between 0 and 2.5°C where the phase partitioning schemes differ.
- The BATS snow albedo parameterization with the default values from the MPTABLE.TBL are too slow in decreasing the snow albedo compared to available observations. This appears to be particularly evident following rain-on-snow events and has potentially large implications for the surface energy balance and the timing of snowmelt and runoff.

References

Albert, M. R., and F. E. Perron Jr. 2000. "Ice Layer and Surface Crust Permeability in a Seasonal Snow Pack." *Hydrological Processes* 14 (18): 3207–14.

Blaylock, B. K., J. D. Horel, and S. T. Liston. 2017. "Cloud Archiving and Data Mining of High-Resolution Rapid Refresh Forecast Model Output." *Computers & Geosciences* 109: 43–50.

Brotzge, J. A., J. Wang, C. D. Thorncroft, E. Joseph, N. Bain, N. Bassill, N. Farruggio, et al. 2020. "A Technical Overview of the New York State Mesonet Standard Network." *Journal of Atmospheric and Oceanic Technology*: 1–48.

Covert, J. M. 2019. *Design and Implementation of the New York State Mesonet Flux Tower Network*. State University of New York at Albany.

Cuntz, M., J. Mai, L. Samaniego, M. Clark, V. Wulfmeyer, O. Branch, S. Attinger, and S. Thober. 2016. "The Impact of Standard and Hard-Coded Parameters on the Hydrologic Fluxes in the Noah-MP Land Surface Model." *Journal of Geophysical Research: Atmospheres* 121 (18): 10–676.

Dickinson, E., A. Henderson-Sellers, and J. Kennedy. 1993. *Biosphere-Atmosphere Transfer Scheme (BATS) Version 1e as Coupled to the NCAR Community Climate Model (No. NCAR/TN-387+STR)*. Boulder, CO: University Corporation for Atmospheric Research. doi:10.5065/D67W6959.

Gochis, D. J., A. Dugger, M. Barlage, K. Fitzgerald, L. Karsten, M. McAllister, J. McCreight, et al. 2018. "The NCAR WRF-Hydro Modeling System Technical Description." NCAR Technical Note. https://ral.ucar.edu/sites/default/files/public/WRFHydroV5TechnicalDescription.pdf.

Harder, P., and J. W. Pomeroy. 2014. "Hydrological Model Uncertainty Due to Precipitation-Phase Partitioning Methods." *Hydrological Processes* 28 (14): 4311–27.

Hedstrom, N. R., and J. W. Pomeroy. 1998. "Measurements and Modelling of Snow Interception in the Boreal Forest." *Hydrological Processes* 12 (10–11): 1611–25.

Iacono, M. J., E. J. Mlawer, S. A. Clough, and J.-J. Morcrette. 2000. "Impact of an Improved Longwave Radiation Model, RRTM, on the Energy Budget and Thermodynamic Properties of the NCAR Community Climate Model, CCM3." *Journal of Geophysical Research: Atmospheres* 105 (D11): 14873–90.

Iziomon, M. G., H. Mayer, and A. Matzarakis. 2003. "Downward Atmospheric Longwave Irradiance under Clear and Cloudy Skies: Measurement and Parameterization." *Journal of Atmospheric and Solar-Terrestrial Physics* 65 (10): 1107–16.

Jennings, K. S., T. S. Winchell, B. Livneh, and N. P. Molotch. 2018. "Spatial Variation of the Rain–Snow Temperature Threshold across the Northern Hemisphere." *Nature Communications* 9 (1): 1–9.

Matonse, A. H., D. C. Pierson, A. Frei, M. S. Zion, E. M. Schneiderman, A. Anandhi, R. Mukundan, and S. M. Pradhanang. 2011. *Hydrological Processes* 25 (21): 3278–88.

Minder, J. R., T. W. Letcher, and S. McKenzie Skiles. 2016. "An Evaluation of High-Resolution Regional Climate Model Simulations of Snow Cover and Albedo over the Rocky Mountains, with Implications for the Simulated Snow-Albedo Feedback." *Journal of Geophysical Research: Atmospheres* 121 (15): 9069–88.

Niu, G.-Y., and Z.-L. Yang. 2007. "An Observation-Based Formulation of Snow Cover Fraction and Its Evaluation over Large North American River Basins." *Journal of Geophysical Research: Atmospheres* 112: D21101.

Niu, G.-Y., Z.-L. Yang, K. E. Mitchell, F. Chen, M. B. Ek, M. Barlage, A. Kumar, et al. 2011. "The Community Noah Land Surface Model with Multiparameterization Options (Noah-MP): 1. Model Description and Evaluation with Local-Scale Measurements." *Journal of Geophysical Research: Atmospheres* 116: D12109.

NOAA (National Oceanic and Atmospheric Administration). 2016. "National Water Model: Improving NOAA's Water Prediction Services." https://water.noaa.gov/documents/wrn-national-water-model.pdf.

Rhoades, A. M., A. D. Jones, and P. A. Ullrich. 2018. "Assessing Mountains as Natural Reservoirs with a Multimetric Framework." *Earth's Future* 6 (9): 1221–41.

Sturm, M., D. K. Perovich, and J. Holmgren. 2002. "Thermal Conductivity and Heat Transfer through the Snow on the Ice of the Beaufort Sea." *Journal of Geophysical Research: Oceans* 107 (C10): SHE-19.

Verseghy, D. L. 1991. "CLASS—A Canadian Land Surface Scheme for GCMs. I. Soil Model." *International Journal of Climatology* 11(2): 111–33.

Wrzesien, M. L., T. M. Pavelsky, S. B. Kapnick, M. T. Durand, and T. H. Painter. 2015. "Evaluation of Snow Cover Fraction for Regional Climate Simulations in the Sierra Nevada." *International Journal of Climatology* 35 (9): 2472–84.

Yang, Z.-L., R. E. Dickinson, A. Robock, and K. Ya Vinnikov. 1997. "Validation of the Snow Submodel of the Biosphere–Atmosphere Transfer Scheme with Russian Snow Cover and Meteorological Observational Data." *Journal of Climate* 10 (2): 353–73.

Yen, Y.-C., K. Cheng, and S. Fukusako. 1991. "A Review of Intrinsic Thermophysical Properties of Snow, Ice, Sea Ice, and Frost." *The Northern Engineer* 24: 53–74.

You, Y., C. Huang, Z.-L. Yang, Y. Zhang, Y. Bai, and J. Gu. 2020. "Assessing Noah-MP Parameterization Sensitivity and Uncertainty Interval Across Snow Climates." *Journal of Geophysical Research: Atmospheres* 125 (4): e2019JD030417.

REPORT DOCUMENTATION PAGE

Form Approved
OMB No. 0704-0188

1. REPORT DATE (DD-MM-YYYY)	2. REPORT TYPE	3. DATES COVERED (From - To)
08/2022	Final Report	

4. TITLE AND SUBTITLE
Understanding and Improving Snow Processes in Noah-MP over the Northeast United States via the New York State Mesonet

5a. CONTRACT NUMBER

5b. GRANT NUMBER

5c. PROGRAM ELEMENT

6. AUTHOR(S)
Theodore W. Letcher, Justin R. Minder, and Patrick Naple

5d. PROJECT NUMBER
NA19OAR4590203

5e. TASK NUMBER

5f. WORK UNIT NUMBER

7. PERFORMING ORGANIZATION NAME(S) AND ADDRESS(ES)
U.S. Army Engineer Research and Development Center (ERDC)
Cold Regions Research and Engineering Laboratory (CRREL)
72 Lyme Road
Hanover, NH 03755-1290

8. PERFORMING ORGANIZATION REPORT NUMBER
ERDC/CRREL TR-22-9

9. SPONSORING / MONITORING AGENCY NAME(S) AND ADDRESS(ES)
National Oceanic and Atmospheric Administration
1401 Constitution Avenue NW, Room 5128
Washington, DC 20230

10. SPONSOR/MONITOR'S ACRONYM(S)
NOAA

11. SPONSOR/MONITOR'S REPORT NUMBER(S)

12. DISTRIBUTION / AVAILABILITY STATEMENT
Approved for public release; distribution is unlimited.

13. SUPPLEMENTARY NOTES

14. ABSTRACT

Snow is a critical component of the global hydrologic cycle and is a key input to river and stream flow forecasts. In 2016, the National Oceanic and Atmospheric Administration launched the National Water Model (NWM) to provide a high-fidelity numerical forecast of streamflow integrated with the broader atmospheric prediction modeling framework. The NWM is coupled to the atmospheric model using the Noah-MP land surface modeling framework. While snow in Noah-MP has been consistently evaluated in the western United States, less attention has been paid to understanding and optimizing its performance in the Northeast US (NEUS). The newly installed New York State Mesonet (NYSM), a network of high-quality surface meteorological stations distributed across New York State, provides a unique opportunity to evaluate Noah-MP performance in the NEUS. In this report, we document the methodology used to perform single-column simulations using meteorological inputs from the NYSM and compare the point evaluations against baseline NWM performance. We further discuss how enhanced surface energy balance measurements at a selection of NYSM sites can be used to evaluate specific components of Noah-MP and present initial results.

15. SUBJECT TERMS
Hydrology; Snow--runoff; Streamflow--Mathematical models; Northeastern States; Meteorology; Meteorologial stations

16. SECURITY CLASSIFICATION OF:			17. LIMITATION OF ABSTRACT	18. NUMBER OF PAGES	19a. NAME OF RESPONSIBLE PERSON
a. REPORT	b. ABSTRACT	c. THIS PAGE			19b. TELEPHONE NUMBER (include area code)
Unclassified	Unclassified	Unclassified	None	50	